

Ag@Nb₂CT_xMXene Composites for Efficient Photocatalytic Degradation of Antibiotics



Submitted by

Javeria Munir

Registration No: 00000403058

A dissertation submitted to the National University of Sciences and Technology, Islamabad in partial fulfillment of requirements for the degree of

Master of Science

In

Physics

Supervised by

Prof. Dr. Syed Rizwan Hussain

Department of Physics

School of Natural Sciences (SNS)

National University of Sciences and Technology (NUST)

Islamabad, Pakistan


THESIS ACCEPTANCE CERTIFICATE

Certified that final copy of MS thesis written by **Javeria Munir** (Registration No. **00000403058**), of **School of Natural Sciences** has been vetted by undersigned, found complete in all respects as per NUST statutes/regulations, is free of plagiarism, errors, and mistakes and is accepted as partial fulfillment for award of MS/M.Phil degree. It is further certified that necessary amendments as pointed out by GEC members and external examiner of the scholar have also been incorporated in the said thesis.

Signature: _____ 

Name of Supervisor: Prof. Syed Rizwan Hussain

Date: 18-09-2024

Signature (HoD): _____ 

Date: 18-09-2024

Signature (Dean/Principal): _____ 

Date: 19-9-2024

National University of Sciences & Technology**MS THESIS WORK**

We hereby recommend that the dissertation prepared under our supervision by: Javeria Munir, Regn No. 00000403058 Titled Ag@Nb₂CTx MXene Composites for Efficient Photocatalytic Degradation of Antibiotics be Accepted in partial fulfillment of the requirements for the award of MS degree.

Examination Committee Members1. Name: PROF. SYED RIZWAN HUSSAINSignature: 2. Name: DR. IMRAN HAIDER SAJIDSignature: Supervisor's Name DR. FAHEEM AMINSignature: Co-Supervisor's Name DR. AAMIR SHAFIQUESignature: 


Head of Department

18-09-2024
Date

COUNTERSIGNEDDate: 19.9.2024


Dean/Principal

DEDICATION

I would want to dedicate this thesis to my Creator, Allah, who has been the guiding force in my life. It is by His support that I have come this far. To my parents, who have always been there for me, offering guidance and inspiration, I dedicate this thesis and my entire academic journey to them.

Acknowledgment

All praise and glory belong to Allah, whose countless blessings and bounties cannot be measured by any mortal. Blessings and Peace be upon the Holy Prophet Hazrat Muhammad (SAW), whose guidance is for the whole of humanity. Alhamdulillah for everything I had and Alhamdulillah for everything I will have. I extend my heartfelt gratitude to my supervisor, Dr. Syed Rizwan Hussain, for his unwavering guidance, advice, and patience throughout every stage of this research. I am deeply thankful to my co-supervisor, Dr. Imran Haider Sajid, for his valuable suggestions and ongoing support during the entire program. My sincere thanks also go to my GEC members, Dr. Faheem Amin and Dr. Amir Shafique, for their insightful advice and suggestions, which greatly contributed to the improvement of my thesis and research work.

I am very thankful to Prof. Dr Rashid Farooq principal SNS and school administration for providing us with resources and a sound environment to research. I am profoundly grateful to all the teachers who have guided me throughout my life, shaping my personality and enabling me to reach the level I am at today. I would also like to express my sincere appreciation to my friends, especially Aiza and Sheryar, for their discussions, guidance, and support, which kept me motivated during my research. Additionally, I acknowledge the efforts and guidance of my senior fellows in the 2D nanomaterials group: Rabia Tahir, Kubra Sattar, Arooma Syed, Aamen Nasir, Lazare, Irfan Bajwa and Nayab Gul. I am thankful to National University of Science and Technology for giving me a platform for my MS in such a prestigious institute. I spent one of the best academic years in this institute under highly qualified faculty members.

Lastly, I want to express my deepest thanks and appreciation to my family (my parents, siblings, uncle, aunt, and cousins and all my well-wishers) for their constant support. Their love and encouragement have meant everything to me, and I will always be grateful to them.

Javeria Munir

Contents

Abstract	ix
Chapter 1	ix
Introduction.....	1
1.1 Introduction to Nanotechnology	1
1.1.1 Introduction to Nanotechnology	1
1.2 Nanomaterials.....	1
1.2.1 Dimensional Classification of Nanomaterials	2
1.3 Water Contamination and Public Health: A Growing Concern.....	2
1.4 Antibiotics	3
1.4.1 Problems Caused by Antibiotics Contaminated Water	3
1.5 Purification Methods	3
1.6 Photocatalysis and photocatalyst.....	4
1.6.1 Photo-catalysis.....	4
1.6.2 Types of Photocatalysis	5
1.6.3 Mechanism of Photocatalysis	5
1.6.4 Types of photocatalysts.....	6
1.6.5 Factors influencing the Photocatalytic Activity.....	7
1.6.6 Applications of Photocatalysts.....	8
Chapter 2.....	10
Literature Review.....	10
2.1 Two-dimensional Materials	10
2.1.1 MAX Phase.....	11
2.1.2 Synthesis of MXene.....	12
2.1.3 Chemical Reactions	13
2.1.4 Factors influencing the Synthesis	14
2.1.5 Methods of Synthesis of MXene	14
2.2 Properties of MXenes.....	16
2.2.1 Mechanical Properties	16
2.2.2 Electronic Properties.....	17
2.2.3 Optical Properties	17

2.2.4 Chemical Properties.....	17
2.2.5 Magnetic Properties.....	17
2.2.6 Thermal Properties.....	18
2.2.7 Photocatalytic Properties	18
2.3 Applications of MXenes.....	18
2.3.1 Energy Storage Applications	19
2.3.2 Biomedical Applications.....	20
2.3.3 Sensors and Membranes	20
2.3.4 Applications of MXenes as Photocatalytic Agents.....	21
2.3.5 Applications of MXenes as Antibacterial Agents.....	22
2.4 Literature Survey of Photocatalytic Activity of MXene and MXene Based Nanocomposites	23
2.4.1 Review of Problem	23
Chapter 3.....	25
Apparatus and Experimental Measurements	25
3.1 Chemicals.....	25
3.2 Apparatus Description.....	25
3.2.1 Digital Weight Balance.....	26
3.2.2 Hot Plate	27
3.2.3 Fume Hood	27
3.2.4 Centrifuge Machine	28
3.2.5 Vacuum Filtration Assembly	28
3.2.6 Vacuum Drying Oven	29
3.2.7 Water Bath Sonicator	29
3.2.8 Halogen Lamp	29
3.3 Characterization Techniques	30
3.3.1 X-Ray Diffraction (XRD).....	31
3.3.2 Scanning Electron Microscope.....	32
3.3.3 Energy Dispersive X-ray Spectroscopy (EDX).....	33
3.3.4 Raman Spectroscopy	34
3.3.5 Fourier Transform Infrared Spectroscopy (FTIR).....	34
3.3.6 Photoluminescence (PL) Spectra.....	35
3.3.7 Ultraviolet-Visible Spectroscopy.....	36

3.3.8 Photocatalytic Measurements	37
Chapter 4	38
Synthesis and Result Analysis	38
4.1 Synthesis Procedure	38
4.1.1 Etching of Nb ₂ AlC MAX	38
4.1.2 Delamination of Nb ₂ C MXene with Isopropyl Amin (i-PrA)	39
4.1.3 Synthesis of Silver Nanoparticles.....	39
4.1.4 Synthesis of Nb ₂ C and Ag-NPs Composite.....	39
4.2 XRD Analysis.....	40
4.2.1 XRD Analysis of etching of Nb ₂ AlC.....	40
4.2.2 XRD Analysis of delaminated MXene using isopropyl amine.....	41
4.2.3 XRD Analysis of Nb ₂ C/Ag-NPs Composite.....	42
4.3 Scanning Electron Microscope (SEM).....	43
4.3.1 SEM Images of MAX and MXene.....	43
4.3.2 SEM Images of Nb ₂ C-Ag NPs composite.....	44
4.4 Energy Dispersive X-Ray Spectroscopy (EDX)	44
4.4.1 EDX of MXene.....	44
4.4.2 EDX of Nb ₂ C-Ag NPs.....	45
4.5 Raman Spectroscopy	45
4.6 Fourier Transform Infrared Spectroscopy (FTIR).....	47
4.7 Photocatalytic Degradation and UV VIS Spectroscopic Analysis	48
4.7.1 Tauc Plot of MXene and Nanocomposites using UV/Vis Spectroscopy	48
4.7.2 Photocatalytic Activity of MXene and Nanocomposites.....	49
4.8 Photoluminescence Spectra Analysis	72
Conclusion	74
Future Perspective.....	75

List of Figures

Figure 1: Dimensional classification of nanomaterials [4].....	2
Figure 2: Strategies to enhance the Photocatalytic activity [18].....	8
Figure 3: Applications of Photocatalysts [18].....	9
Figure 4: Categories of 2D materials [19].....	11

Figure 5: MAX phases $Mn+1AX_n$ forming elements [21].....	12
Figure 6: Synthesis of MXene [25].....	13
Figure 7: Classification of Top-Down Approach.....	15
Figure 8: Classification of Bottom-Up Approach.....	15
Figure 9: Applications of MXenes [36].	19
Figure 10: Applications of MXenes in Biomedical Field [38].	20
Figure 11: MXenes Applications in Sensors [43].	21
Figure 12: Applications of MXenes as Photocatalytic Agents [45].	22
Figure 13: Antibacterial Activity of MXenes [46].	22
Figure 14: Digital Weight Balance.....	27
Figure 15: Hot Plate.....	27
Figure 16: Fume Hood [55].	28
Figure 17: Vacuum Drying Oven.....	29
Figure 18: Halogen Lamp.	30
Figure 19: Phenomenon of Bragg's Law Conditions [56].	31
Figure 20: Schematic diagram of Scanning Electron Microscope [57].	32
Figure 21: Generation of X-Rays [58].	33
Figure 22: Raman spectroscopy schematic [59].	34
Figure 23: Working of FTIR spectrometer [60].	35
Figure 24: Working of Photoluminescence (PL) Spectra [61].	36
Figure 25: Double Beam Spectrophotometer [62].	37
Figure 26: Synthesis of Nb ₂ CT _x MXene.	38
Figure 27: Synthesis of Nb ₂ CT _x MXene/Ag NPs Composite.	40
Figure 28: XRD Analysis of MAX and MXene.	41
Figure 29: XRD analysis of MAX, MXene and delaminated MXene.....	42
Figure 30: XRD Analysis of MXene and Mxene/Ag NPs composite.	43
Figure 31: SEM Images of (a) Nb ₂ AlC MAX at 10 μ m, (b) and (c) Pristine Nb ₂ CT _x MXene at 5 μ m and 1 μ m respectively.	44
Figure 32: SEM Images of (a), (b) and (c) Nb ₂ CT _x /Ag NPs composite at 5 μ m, 1 μ m and 0.5 μ m respectively.	44
Figure 33: (a)EDX analysis of MXene and (b) MXene/Ag NPs composite.....	45
Figure 34: (a) Raman spectra of MAX and MXene (b)MXene and Composite (c) deconvoluted spectra of Nb ₂ CT _x /Ag NPs composite.....	46
Figure 35: FTIR analysis of MXene and composite.....	47
Figure 36: Band gap of (a) MXene (b) C1 (c) C2 (d) C3	49
Figure 37: Photocatalytic Activity Testing.....	50
Figure 38: UV/Vis Spectra of 10ppm antibiotic solutions of (a) Norfloxacin (b) Fleroxacin.....	51
Figure 39: Photocatalytic degradation by Pristine MXene case 1.	52
Figure 40: Photocatalytic degradation by pristine MXene case 2.	53
Figure 41: Photocatalytic degradation by pristine MXene case3.	53
Figure 42: Photocatalytic degradation by C1 case 1.....	54
Figure 43: Photocatalytic degradation by C1 case 2.....	55
Figure 44: Photocatalytic degradation by C1 case 3.....	56

Figure 45: Photocatalytic degradation by C2 case 1.....	57
Figure 46: Photocatalytic degradation by C2 case 2.....	57
Figure 47: Photocatalytic degradation by C2 case 3.....	58
Figure 48: Photocatalytic degradation by C3 case 1.....	59
Figure 49: Photocatalytic degradation by C3 case 2.....	60
Figure 50: Photocatalytic degradation by C3 case 3.....	60
Figure 51: Kinetic studies of MXene and nanocomposites (a) with 3mg (b) with 15mg (c) with 30mg.	61
Figure 52: Photocatalytic degradation by pristine MXene case 1.	63
Figure 53: Photocatalytic degradation by pristine MXene case 2.	63
Figure 54: Photocatalytic degradation by pristine MXene case 3.	64
Figure 55: Photocatalytic degradation by C1 case 1.....	65
Figure 56: Photocatalytic degradation by C1 case 2.....	66
Figure 57: Photocatalytic degradation by C1 case 3.....	66
Figure 58: Photocatalytic degradation by C2 case 1.....	67
Figure 59: Photocatalytic degradation by C2 case 2.....	68
Figure 60: Photocatalytic degradation by C2 case 3.....	68
Figure 61: Photocatalytic degradation by C3 case 1.....	69
Figure 62: Photocatalytic degradation by C3 case 2.....	70
Figure 63: Photocatalytic degradation by C3 case 3.....	70
Figure 64: Kinetic studies of MXene and nanocomposites (a) with 3mg (b) with 15mg (c) with 30mg.	71
Figure 65: PL Spectra of Pristine MXene and nanocomposites.	72

Abstract

Medicines are crucial for our health, but the discharge of untreated wastewater containing antibiotics by pharmaceutical industries into reservoirs even at low concentration and their degraded products can lead to serious issues such as skin cancer, allergies, and other diseases. Addressing this environmental concern is essential for the well-being of both human and the planet. Research on two-dimensional materials, driven by their remarkable properties, has led to the discovery of MXenes. These 2D materials, with their large surface area, tunable electronic structure, and excellent conductivity, make effective photocatalysts by enhancing light absorption and charge separation. In this study, silver nanoparticles (Ag NPs), known for their antimicrobial and catalytic properties, were incorporated into MXene sheets to enhance their capabilities for applications such as antibiotic degradation in water purification. The MXene/Ag NPs composites were synthesized by a cost effective and simple self-assembly electrostatic method, characterized, and evaluated, showing superior photocatalytic activity compared to pure MXene. This improved degradation efficiency is due to reduced charge recombination in the nanocomposites. The synthesized nanocomposites show strong potential for catalytic applications.

Chapter 1

Introduction

1.1 Introduction to Nanotechnology

This section covers the introduction to nanotechnology and nanomaterials, including their dimensional classification with a focus on two-dimensional nanomaterials. It then provides a detailed discussion on MAX phases and MXenes.

1.1.1 Introduction to Nanotechnology

In nanotechnology, atoms and molecules are reduced in size and manipulated to change their physical properties, like chemical reactivity, conductivity, and strength. This is important because nanotechnology can be used in many areas, such as biotechnology, electronics, medicine, optics, and electrical devices. Because of this, researchers are studying the basic features of nanomaterials in depth. Nanotechnology is a fast-growing field that can improve many synthesis methods and their applications. Nanotechnology can create new opportunities in mechanical, electrical, medicinal, and agricultural engineering, as well as in the food and agriculture industries. Ongoing research in nanotechnology and nanomaterials, where materials exhibit unique properties at the nanoscale, could enhance the service life and reduce the costs of building infrastructure, transforming industries and creating new opportunities[1].

1.2 Nanomaterials

The advent of nano-sized items or materials with dimensions in the nanoscale range has greatly enhanced the efficiency of various commonly used devices in our era of scientific progress. Nanomaterials are of greater interest at the nanoscale due to the emergence of unique optical, magnetic, electrical, and other properties. These new properties can have big effects in different areas like electronics and medicine and beyond[2]. Advances in material synthesis have led to the categorization of materials into 0-D, 1-D, 2-D, and 3-D nanomaterials when considered in bulk. Nanomaterials form the fundamental components of nanotechnology, with materials having at least one dimension less than 100 nm classified as nanoscale materials ($1 \text{ nm} = 1 \times 10^{-9} \text{ m}$, roughly one hundred thousand times smaller than the diameter of a human hair).

1.2.1 Dimensional Classification of Nanomaterials

Nanomaterials are categorized based on the number of dimensions limited to the nano scale, such as 0- dimensional, 1-dimensional, 2-dimensional and 3-dimensional structures. Materials like quantum dots and nanostructures fall into the 0D category when all their physical dimensions are within the 0-100nm range. Nanorods, wires and similar structures are considered 1D nanomaterials if one dimension extends beyond the 100nm range. On the other hand, nanoclusters and traditional materials with dimensions exceeding 100nm are classified as 2D and 3D nanomaterials, respectively[3].

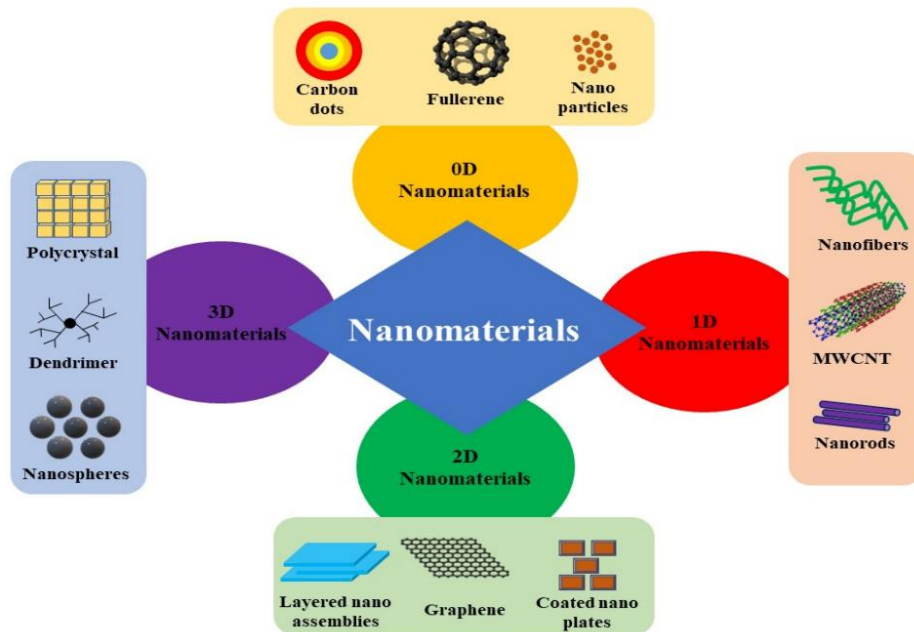


Figure 1: Dimensional classification of nanomaterials[4].

1.3 Water Contamination and Public Health: A Growing Concern

Water is essential to human civilization, covering about 71% of the Earth's surface. However, 97% of it is saltwater, 2% is frozen, and only 1% is consumable. This small fraction must meet the demands for consumption, household chores, and industrial applications, but it is unevenly distributed. Despite the abundance of water on Earth, the available freshwater is insufficient due

to rapid population growth and industrialization, leading to a global water crisis. Natural water sources often contain heavy textile and pharmaceutical contaminants, making them unsafe for direct consumption and posing risks to human and environmental health[5],[6]. While medicines are crucial for our health, the discharge of untreated wastewater containing antibiotics even at low concentration and their degraded products can lead to serious issues such as skin cancer, allergies, and other diseases. If this contaminated water can enter drinking water supplies, leading to human exposure to antibiotics. Long-term exposure to low levels of antibiotics in drinking water may contribute to the development of antibiotic resistance in humans and could have other unknown health effects. It is imperative to address and treat this environmental concern for the well-being of both people and the planet.

1.4 Antibiotics

Antibiotics are utilized to treat or prevent certain bacterial infections by either killing the bacteria or inhibiting their spread. However, they are not effective against everything. Many minor bacterial infections can resolve on their own without the need for antibiotics. Antibiotics are ineffective against viral infections like colds, flu, and most coughs.

1.4.1 Problems Caused by Antibiotics Contaminated Water

The presence of emerging contaminants in water poses significant risks to human health. Exposure to pharmaceutical residues can lead to adverse health effects, such as endocrine disruption, antibiotic resistance, skin cancer and skin allergies to both human and aquatic life. The spread of waterborne diseases like cholera and typhoid already pose considerable health risks, and the presence of emerging contaminants can worsen these issues. This highlights the urgent need for improved water quality management[7]

1.5 Purification Methods

There are different water treatment technologies, which have been reported and are of great practical significance to remove diverse pollutants from wastewater. The water purified by advance purification techniques provides high-quality consumable water. Advanced purification methods include[6]

- Microfiltration/ultrafiltration/nanofiltration
- Membrane separation

- Adsorption
- Reverse osmosis
- Sedimentation
- Solar disinfection
- Aeration
- Chemical disinfection
- Advanced oxidation
- Photocatalysis.

Notably, photocatalysis is an effective method for dye, organic and antibiotics degradation because of its advantages, such as its eco-friendliness, high efficiency, low cost, and reusability.

1.6 Photocatalysis and photocatalyst

Among various water treatment technologies, photocatalysis is considered as an advanced technology known for environmental cleanliness and plays a crucial role in finding sustainable solutions to global and environmental challenges.

1.6.1 Photo-catalysis

Photocatalysis derives from the Greek words' "photo" meaning "light" and "catalysis" meaning "to decompose or break apart." It is a process that uses light to activate a substance known as a Photocatalyst, which modifies a chemical reaction without undergoing any chemical transformation itself, allowing it to be used repeatedly for catalysis.

Unlike thermal catalysts, which are activated by heat, photocatalysts are activated by photons with appropriate energy. Upon absorbing these photons, a photocatalyst generates electron-hole pairs that degrade pollutants into less toxic materials. An example of a natural photocatalyst is chlorophyll, which converts CO₂ and H₂O into glucose and oxygen[8]. Photocatalysis is crucial for addressing energy and environmental crises. Commonly used photocatalysts for environmental remediation include semiconductor photocatalysts. These materials absorb solar energy, generating electron-hole pairs, which then oxidize and reduce toxic environmental pollutants, converting them into CO₂ and H₂O. An ideal photocatalyst has a large surface area, a suitable band-gap, an appropriate morphology, and can be reused[9].

1.6.2 Types of Photocatalysis

There are two types of photocatalysis.

1. Homogeneous Photocatalysis

2. Heterogeneous Photocatalysis

1.6.2.1 Homogeneous Photocatalysis

When reactants and a photocatalyst are in same phase, it is known as homogeneous photocatalysis. Commonly used homogeneous photocatalysts include photo-Fenton systems and ozone[10]. Homogeneous photocatalysis is a highly effective method for degrading organic pollutants, offering significant advantages in reaction rates and simplicity of reactor design, though challenges remain in catalyst recovery and process optimization.

1.6.2.2 Heterogeneous Photocatalysis

Heterogeneous photocatalysis occurs when the reactants and the photocatalyst are in different phases. In this process, an interface forms between the solid photocatalyst and the liquid or gas containing the products. Typically, the solid photocatalyst consists of a semiconductor material that absorbs photons when illuminated by visible light. Photocatalytic oxidation and reduction reactions take place at the interface between the gas or liquid phase and the semiconductor photocatalyst. Heterogeneous photocatalysis is widely used in energy and environmental applications, as well as in organic synthesis[11]. Organic waste gets converted into less toxic substances through photocatalysis. Heterogeneous photocatalysis is a cost-effective method for the degradation of environmental and organic pollutants[12].

1.6.3 Mechanism of Photocatalysis

When a photon with energy equal to or greater than the band-gap energy of the photocatalyst is absorbed by the material, an electron is excited from the valence band to the conduction band. The generation of photogenerated charge carriers is a crucial step in all photocatalytic processes. Electrons - holes pairs tries to recombine, releasing energy in the form of heat. However, an electric field forms at the semiconductor-fluid interface, reducing the recombination rate. This increases the lifetime of the charge carriers, allowing charge transfer between species and initiating a chemical reaction. Interfacial electron transfer, which involves the movement of electrons between the contaminated solution and the semiconductor photocatalytic material, is the most crucial step in the photocatalytic process. This transfer initiates redox reactions, leading to the formation of the

desired products[13]. The three primary steps of semiconductor photocatalysis can be outlined as follows:

- Excitation of electrons from the valence band (VB) to the conduction band (CB) due to solar energy absorption.
- Migration of the generated charge carriers to the surface of the photocatalyst.
- Interaction of the transferred electrons/holes with adsorbed electron acceptors and donors[14].

A significant challenge in the second step is the increased recombination of charge carriers. To address this issue, several strategies are employed to control or reduce the recombination of photogenerated charge carriers.

1.6.4 Types of photocatalysts

The energy difference between the conduction band and valence band is known as the "band gap." Photocatalysts are classified into three categories based on their band gap values:

- **Metal Photocatalysts:** These have a band gap of less than 1 eV.
- **Semiconductor Photocatalysts:** These have a band gap ranging from 1.5 to 3.0 eV.
- **Insulator Photocatalysts:** These have a band gap greater than 5.0 eV.

Semiconductor based Nanomaterial (Photocatalyst)

Semiconductor nanomaterials are emerging materials in photocatalytic applications due to their unique physical and chemical properties. Various types of semiconductors, like metal oxides, nitrides, chalcogenides, and carbon nitride, are used for dyes and organic pollutants. Challenges in this field include efficient charge separation and maximizing visible light absorption. Nanostructured semiconductors show enhanced activity due to increased surface area and active sites, but their small size can lead to increased recombination rates and decreases photocatalytic degradation. Formation of heterostructures greatly decreases the rate of recombination[15]. A good photocatalytic system needs the right band-gap, a large surface area, the ability to be reused, durability, and the right shape. Metal oxides such as chromium, vanadium, zinc, and cerium are commonly used for breaking down dyes using light. When light is absorbed, it splits apart charges.

The positive charges (holes) then break down harmful dyes and organic pollutants by reacting with them.

The photocatalytic effectiveness of semiconductor materials relies on two factors:

- Producing hydroxyl radicals through the oxidation of hydroxyl anions.
- Creating oxygen radicals through the reduction of oxygen.

Well-studied semiconductor photocatalysts such as TiO_2 , SnO_2 , CeO_2 , and ZnO have been widely employed for breaking down dyes like methyl blue, methylene orange, Rhodamine blue, Congo red and organic pollutants[16].

Metal Oxides as Photocatalyst

Commonly used metal oxides for the degradation of organic pollutants include TiO_2 , ZnO , MoO_3 , SnO_2 , SiO_2 , ZnS , and CoO . These metal oxides can absorb energy in the UV, Visible region, or both. When irradiated with sunlight, electrons gain energy and move from the valence band to the conduction band, leaving behind holes. These charge carriers are responsible for degrading environmental pollutants.

Polymers Used as Photocatalyst

Several organic and inorganic polymers, along with metal oxide nanoparticles, have been reported for the photocatalytic degradation of toxic azo dyes. Currently, g-C₃N₄ is a widely used organic polymer for photocatalytic applications. Zhang et al. reported a ZnO layered hydroxide @ graphitic carbon nitride nanocomposite, synthesized by the co-precipitation method. Using ZnO/g-C₃N₄, 90% of methylene blue (MB) was degraded after five cycles under UV-VIS irradiation[17].

1.6.5 Factors influencing the Photocatalytic Activity

Regulating the energy band structures is the most effective method to enhance visible light photocatalytic performance. This can generally be achieved through doping, defect engineering, and surface modification.

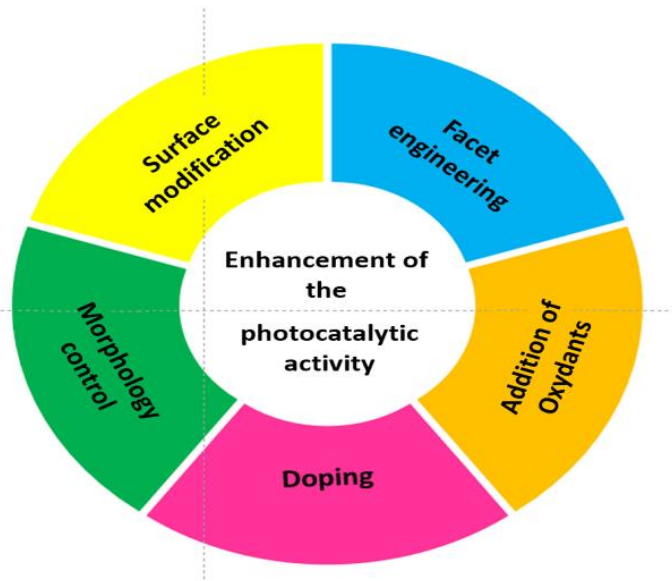


Figure 2: Strategies to enhance the Photocatalytic activity [18].

1.6.6 Applications of Photocatalysts

Photocatalysts have a wide range of applications, including energy storage, odor removal, self-cleaning, sterilization, air purification, and wastewater treatment. They also prevent fouling and fogging of surfaces. Semiconductor-based photocatalysts are particularly effective as sensitizers in light-assisted oxidation and reduction reactions due to their electronic band structure and behavior of electrons. These photocatalysts can completely degrade various toxic environmental contaminants such as dyes, pesticides, insecticides, and antibiotics in water.

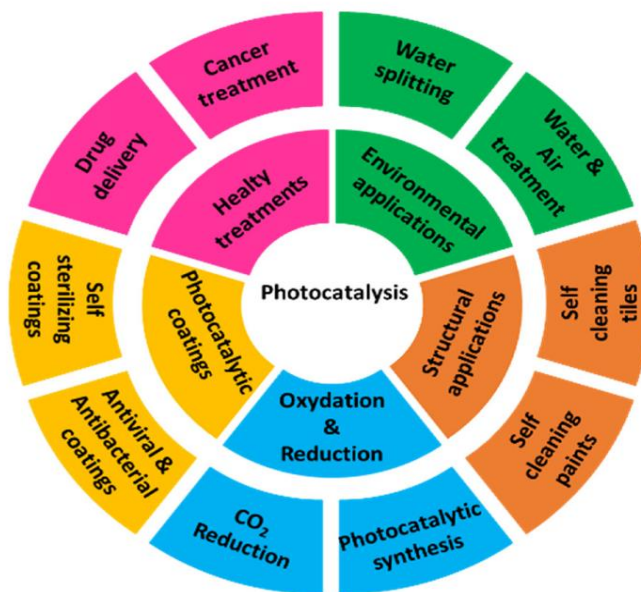


Figure 3: Applications of Photocatalysts [18].

Chapter 2

Literature Review

This section provides the concise information on the two-dimensional materials, MAX phases and synthesis of 2D MXene through HF etching, followed by the synthesis of MXene-based nanocomposites as photocatalysts. Extensive research has been conducted on the photocatalytic properties of MXenes. In this study, we investigate the photocatalytic properties of MXenes by conducting experiments to assess their effectiveness against antibiotics and dyes.

2.1 Two-dimensional Materials

In an era of scientific development, the introduction of nano-level objects (materials having one or two dimensions in the nanometer range) has improved the efficiency of many daily used devices. These materials have tremendous effects in the fields of biomedical, electronics, thermodynamics, optics, materials science, etc. The advancement in the field of material synthesis has categorized material to be 0-Dimensional, 1-Dimensional, 2-Dimensional, and bulk to be 3-Dimensional nanomaterials.

As the name suggests, 2D materials are a type of nanomaterial with a maximum of two dimensions outside the nanometer range (i.e., thickness < 100 nm, with length and width > 100 nm). Examples of 2D materials include thin films, nanosheets, and multi-layered coatings. The properties and behavior of materials are primarily influenced by their size, and as the size decreases, their chemical, electrical, and mechanical properties are greatly enhanced.

Since the discovery of Graphene in 2004, scientists have extensively researched its various aspects, fascinated by its remarkable properties and stability in forming single-carbon atom thick networks as continuous carbon polygons. Subsequently, a range of other carbon-based 2D allotropies such as graphyne, graphdiyne, and graphene dodecagons have also been investigated. Additionally, the study of Graphene has led to the exploration of other forms of 2D materials like transition metal dichalcogenides (TMDs), phosphene, and hexa-boron nitrate.

As previously mentioned, 2D nanomaterials encompass a class of materials where at least two physical dimensions are within the nanometer range. This category includes transition metal dichalcogenides (TMDs), phosphene, and hexa-boron nitrate, which have emerged from the

research on Graphene. These 2D materials possess the unique ability to exfoliate and form layered structures, resulting in improved electrical, optical, mechanical, and thermal properties.

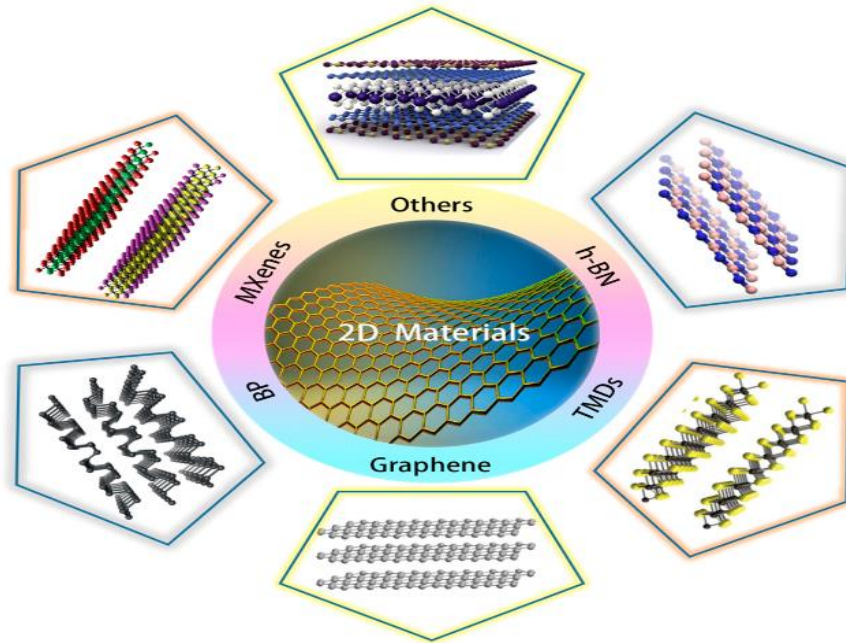


Figure 4: Categories of 2D materials [19].

2.1.1 MAX Phase

MAX phases are a class of layered ternary compounds that exhibit a unique combination of metallic and ceramic properties. These compounds consist of a transition metal (M), an "A-group" element (typically from groups IIIA to VIA of the periodic table, denoted as "A"), and carbon or nitrogen (X), arranged in a hexagonal or trigonal lattice. Each unit cell of a MAX phase contains two formula units, where $M_{n+1}X_n$ layers are sandwiched with pure A-element layers. In simpler terms, closely packed M layers are interspersed between A layers, with C atoms occupying the octahedral sites within the M layers. The general formula for MAX is $M_{n+1}AX_n$, where M belongs to transition metals (i.e. Nb, Ti, V, Ta, Hf, Mo, etc.), X represents carbon or nitrogen, and n is an integer (1-4)[20]. Separating the $M_{n+1}X_n$ layers from the A layers through shearing is challenging due to metallic bonding, but the M-A bonds are more chemically reactive than the M-X bonds, allowing for exfoliation via chemical reactions. Selective etching in dilute fluoride-containing acid results in a stack of $M_{n+1}X_n$ 2D layers. MAX phases have earned significant attention due to their high melting points, excellent thermal conductivity, and good mechanical stability. They can be machined and shaped like metals while exhibiting properties similar to

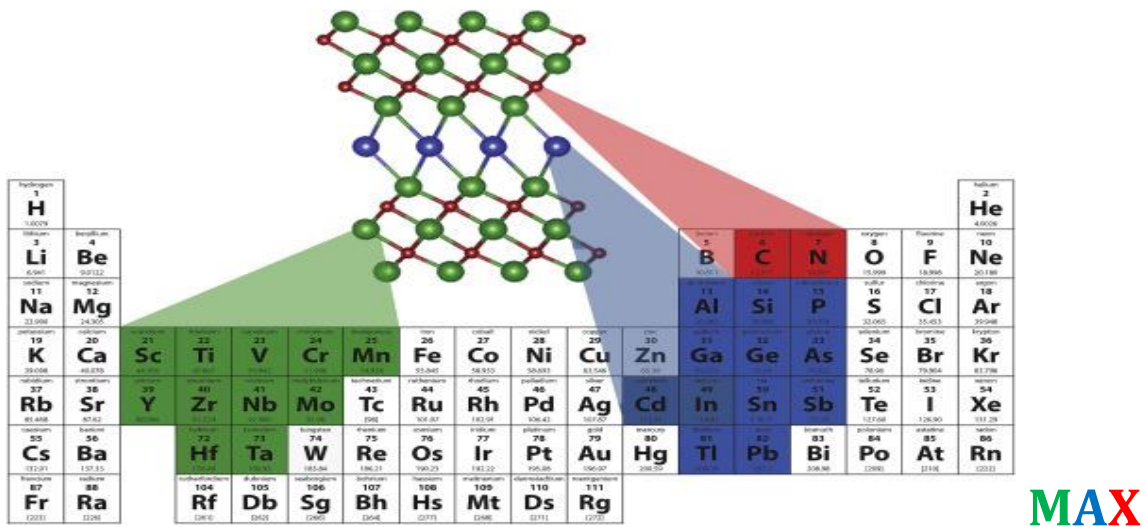


Figure 5: MAX phases $M_{n+1}AX_n$ forming elements[21].

ceramics. Additionally, MAX phases are known for their outstanding oxidation resistance and thermal shock resistance, making them suitable for use in extreme environments. Till January 2022, there are approximately 70 known MAX phases. Most of these phases were synthesized by Wolfgang Jeitschko and Hans Nowotny in the early 1960s, during which they prepared nearly 100 new carbides and nitrides.

2.1.2 Synthesis of MXene

Since 2004 discovery of graphene opened a new window of advancement. Recently Two-dimensional (2D) nanomaterial $Ti_3C_2T_x$ MXene was first discovered in 2011 by Yury Gogotsi and their collaborators. MXenes are produced by selectively etching specific atomic layers from their layered precursors, known as MAX phases. These phases contain a large family of ternary carbides and nitrides, including a wide array of ordered double transition metal structures and solid solutions. MAX phases are composed of layers of transition metal carbides or nitrides ($M_{n+1}X_n$) embedded with layers of A-element atoms ($M_{n+1}AX_n$), typically from groups 13 and 14 of the periodic table. Because the M-X bond is metallic, it has not been possible to physically shear MAX phases to separate the $M_{n+1}X_n$ layers and form MXenes.

However, it is possible to selectively etch A layers because M-A bonds are more chemically active than the stronger M-X bonds. Highly selective etching is essential for producing MXenes. The first

successful etching of an MXene resulted in the creation of Ti_3C_2 from its parent Ti_3AlC_2 MAX phase[22].

It's also important to note that altering the MXene manufacturing process can lead to significant variations in surface group concentrations. For example, surface groups produced by HF or HCl/LiF etching are primarily composed of -O, -OH, and -F groups. Nuclear magnetic resonance (NMR) spectroscopy was used to examine the concentrations of various terminations on HF and HCl/LiF-synthesized $Ti_3C_2T_x$ MXene. It was reported that HF-synthesized MXene had more -OH and fewer -O terminations compared to pure $Ti_3C_2T_x$ MXene generated using HCl/LiF, along with roughly four times as many -F groups. Additionally, when varying HF concentrations are used in the same procedure, the surface terminal composition can change[23]. Specifically, the concentration of -F surface terminations increase as the amount of HF solution per gram of MAX phase is increased.

2.1.3 Chemical Reactions

The synthesis of MXene is assumed to involve the following processes[24]:

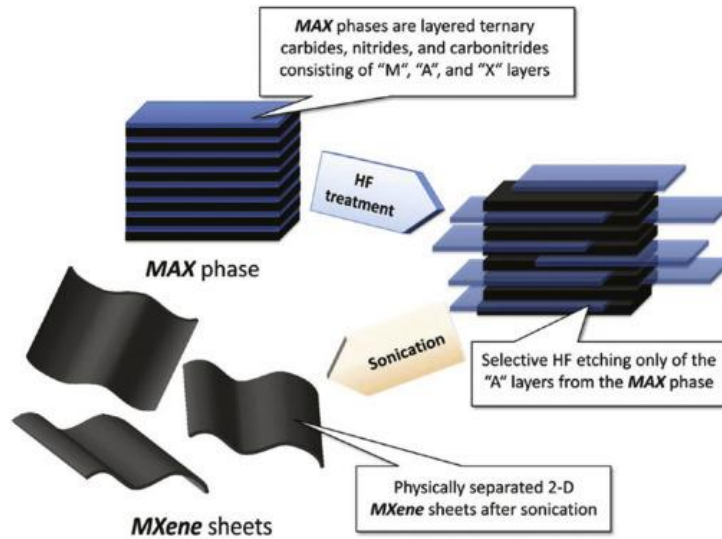
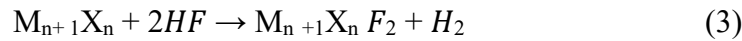
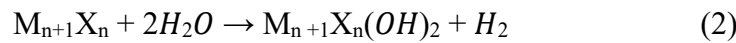
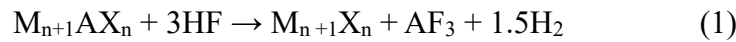


Figure 6: Synthesis of MXene [25].

These equations suggest that an element of the MAX phase reacts with the fluorine in HF to form $M_{n+1}X_n$, which then further reacts with HF and H_2O to produce surface functional groups[23]. Through multiple washes with deionized (DI) water until the pH is neutral, the AF_3 generated in these reactions can be removed.

2.1.4 Factors influencing the Synthesis

The synthesis of MXene is influenced by several factors[26]:

1. Etching time
2. Different HF concentrations
3. Sizes of the corresponding MAX phase powder particles
4. Temperature

Researchers suggest that the binding energies of the M-Al bonds and the variety of M and A components directly affect the etching conditions. These factors are utilized to improve the quality of MXene, reduce the etching time, and increase the yield. Variations in the M and A elements, along with changes in the binding energies of the M-Al bonds, play a crucial role in optimizing the etching process to achieve better MXene quality, shorter etching times, and higher yields.

2.1.5 Methods of Synthesis of MXene

There are two methods of synthesizing 2D MXenes which are as follows:

- 1 Top-Down Approach
- 2 Bottom-Up Approach

2.1.5.1 Top-Down Approach

In this procedure, large quantities of bulk material are exfoliated either mechanically or chemically to produce MXene[27]. By disrupting the van der Waals interactions between the M and A layers, single-layered structures can be created from the bulk material in a controlled manner. This top-down approach is also cost-effective.

Classification of Top-Down Approach

Top-Down approach is classified as

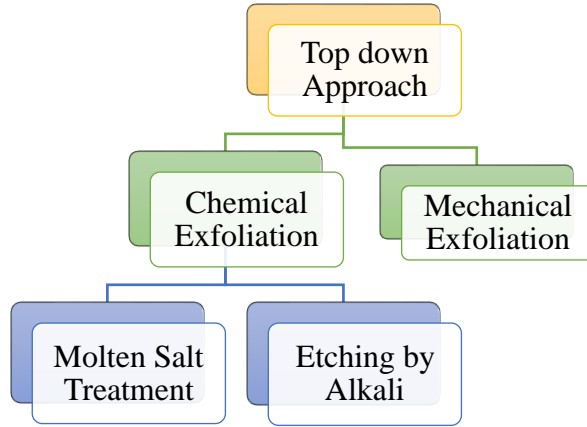


Figure 7: Classification of Top-Down Approach

2.1.5.2 Bottom-Up Approach

This method is essential to create single-layer structures through chemical vapor deposition or hydrothermal processes. These structures can also be produced via etching techniques, with sizes ranging from tens to hundreds of nanometers. This approach is used for large-scale production of 2D materials. The MXenes produced are larger, reaching up to 100 nm[28].

These strategies can be further categorized into two types:

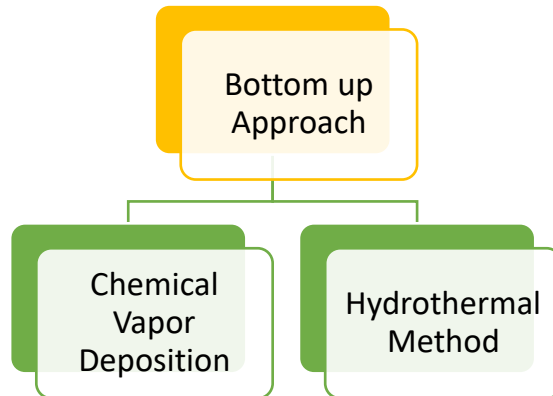


Figure 8: Classification of Bottom-Up Approach

2.2 Properties of MXenes

Since the discovery of MXenes, extensive theoretical and experimental research has been conducted to better understand their physical and chemical properties. MXenes are becoming increasingly desirable in various sectors, including material science and nanotechnology, due to their unique characteristics. They possess superior chemical, electrical, mechanical, physical, and structural qualities, leading to significant advancements in numerous scientific and technological fields. Researchers worldwide are interested to MXenes because of their 2D layered structure's biocompatibility, large adjustable electrical band gap, metallic nature, high Young's modulus, and diverse thermal and electrical properties[29].

The properties of MXenes include:

1. Mechanical Properties
2. Electronic Properties
3. Optical Properties
4. Chemical Properties
5. Magnetic Properties
6. Thermal Properties
7. Photocatalytic properties

2.2.1 Mechanical Properties

Researchers closely study MXenes due to their unique mechanical properties, which vary with surface size. MXenes are becoming attractive materials due to their outstanding flexibility, electrical conductivity, multilayered structures, and strength. The functional groups attached to MXenes significantly impact their stiffness, with MXenes containing -O groups being stiffer than those with -OH and -F groups. The tensile structure linking the layers contributes to their surface flexibility. MXenes' excellent mechanical ion absorption capabilities make them suitable for use in sensors and flexible electronics. Additionally, the number of layers significantly affects their mechanical properties[30]

2.2.2 Electronic Properties

MXenes' most significant electronic characteristic is their excellent electrical conductivity. Their electronic properties are influenced by their metallic nature, thickness, insulation, and surface area[31]. Variations in the band gap of MXenes also alter their electronic activity. Additionally, surface functional groups impact both heat and electrical transport in MXenes[32]. The strong conductivity resulting from their metallic nature makes MXenes ideal for use in supercapacitors and batteries.

2.2.3 Optical Properties

The bandgap of MXenes determines their optical properties. Additionally, the number of MXene layers and the surface functionalization used during experimental synthesis have an impact. Increasing the thickness of MXene films or incorporating ions can alter their optical characteristics[32]. Fluoride and hydroxyl terminations reduce absorption and reflectance in the visible range, while all terminations increase reflectivity compared to pristine MXene. $Ti_3C_2T_x$ films, with a thickness of 5 nm, can absorb light in the UV-Vis region between 300 and 500 nm. This makes them desirable for applications such as photovoltaic devices and transparent conducting electrodes, where absorption of visible and ultraviolet light is beneficial[31].

2.2.4 Chemical Properties

Similar to MXene, titanium carbide ($Ti_3C_2T_x$) can oxidize in the presence of oxygen to form titanium dioxide nanocrystals, which then link together to create an amorphous carbon sheet. Additionally, it can react with oxygen to form the rutile and anatase phases of titanium dioxide[33].

2.2.5 Magnetic Properties

A range of magnetic characteristics are observed in 2D MXene layers. Some MXenes, such as Cr_2C , Ta_3C_2 , and Cr_2N , exhibit ferromagnetic behavior, while others, like Ti_3C_2 and Ti_3N_2 , display antiferromagnetic behavior. Cr_2NT_x and Cr_2CT_x show ferromagnetic properties at room temperature due to the presence of -OH and -F terminations. However, the magnetic moment values for these MXenes have only been theoretically predicted; no practical observations have been made yet[32].

2.2.6 Thermal Properties

Theoretical investigations indicate that MXene exhibits higher thermal conductivity and a lower thermal expansion coefficient compared to other 2D materials. As the number of M atoms increases, the thermal conductivity of M_2CO_2 (where M = Ti, Zr, Hf) also increases. Additionally, all three MXenes demonstrate significant carrier mobility[34].

2.2.7 Photocatalytic Properties

MXenes demonstrate excellent photocatalytic properties due to their tunable electronic structure, which enables efficient electron-hole pair separation and transfer. The presence of surface functional groups enhances stability and provides active sites for reactions. Their layered structure aids in reactant/product diffusion and offers a large surface area. MXenes absorb light across the visible and ultraviolet spectrum, utilizing solar energy effectively. Their metallic conductivity facilitates electron transfer, reducing recombination rates. Band gap engineering and synergistic effects with other materials further optimize their photocatalytic performance. These attributes make MXenes promising for applications such as water splitting, pollutant degradation, and CO_2 reduction. The advantages of Ti_3C_2 MXenes in developing highly efficient photocatalysts are explored, covering their functions as electronic acceptors, substrates, light harvesters and co-catalysts[35].

2.3 Applications of MXenes

MXene is particularly attractive for meeting the energy needs of a growing population due to its diverse and unique features. As a result, there is a high demand for renewable energy storage solutions like batteries and supercapacitors. MXenes are also widely used in various other applications, including absorbents, water filtration, biosensing, hydrogen storage, as well as antibacterial, biomedical and degradation applications[36]. Here are some of the most common uses of MXenes:

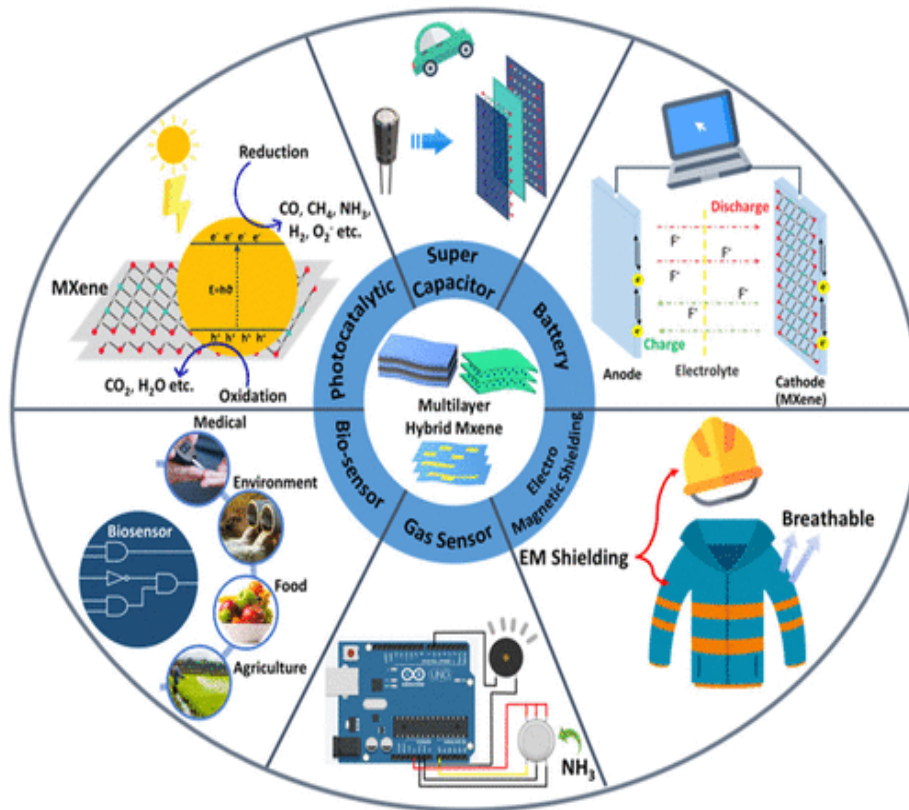


Figure 9: Applications of MXenes [37].

2.3.1 Energy Storage Applications

Although MXenes are utilized in various fields, a significant portion of research focuses on their energy storage capabilities. The metallic core of MXenes enables rapid electron transport, enhancing their ability to store charge efficiently at high rates. Additionally, the metal oxide-like surface provides redox-active sites for pseudocapacitive charge storage, increasing the overall effectiveness of MXenes in energy storage devices such as ultracapacitors and batteries. Furthermore, the sub-nanometer interlayer spacing between the 2D layers allows for swift ion intercalation and diffusion, and these layers can be pre-intercalated with various ions to further boost their storage capacity.

2.3.2 Biomedical Applications

Due to their complete metal atomic layers, variable composition, and hydrophilicity, MXenes have earned more attention from researchers compared to other 2D materials such as hexagonal boron nitrides (h-BN) and graphene.

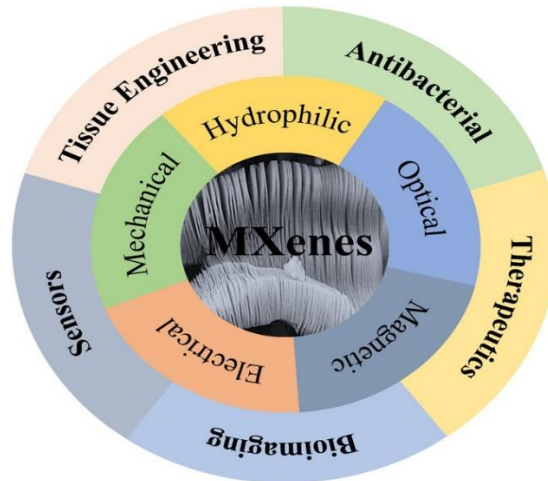


Figure 10: Applications of MXenes in Biomedical Field [38].

MXenes offer a wider range of functional groups and more flexible surfaces than typical 2D materials. They are also used in agriculture and nanoscale drug delivery systems, which distribute medications to various parts of the human body, making them ideal for biological applications such as bioimaging, biosensing, drug delivery, tissue engineering, and antibiotic administration[38].

2.3.3 Sensors and Membranes

MXenes are excellent building blocks for high-performance electrochemical sensors due to their high hydrophilicity, good ion intercalation properties, ease of functionalization, abundance of surface functional groups, strong electrical conductivity, and ease of mass production[39]. They can detect gas noise at concentrations between 50 and 100 ppb at room temperature[40]. Additionally, MXenes are used in biological detection and environmental analysis, including enzyme, gas, and cell absorption detection. They offer broad absorption sites, good dispersion in aqueous solutions, and high metal conductivity[41].

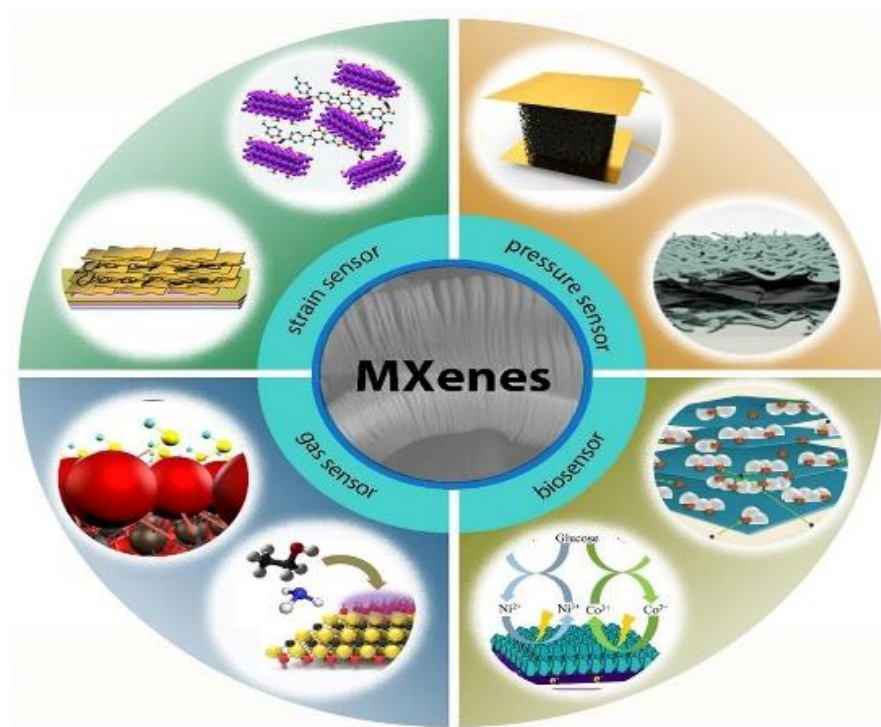


Figure 11: MXenes Applications in Sensors [42].

2.3.4 Applications of MXenes as Photocatalytic Agents

The use of MXene in photocatalysis, including applications such as photocatalytic hydrogen (H₂) production, CO₂ reduction, pollutant degradation and nitrogen (N₂) fixation has been thoroughly investigated. Till date, over 20 types of MXene materials have been identified, though only a limited number such as Ti₃C₂, Nb₂C, Mo₂C, and Ti₂C, are widely used for photocatalysis. Many MXene materials serve as co-catalysts and are combined with numerous photocatalytic semiconductors, including metallic oxides and sulfides and g-C₃N₄, enhancing photocatalytic activity[43].

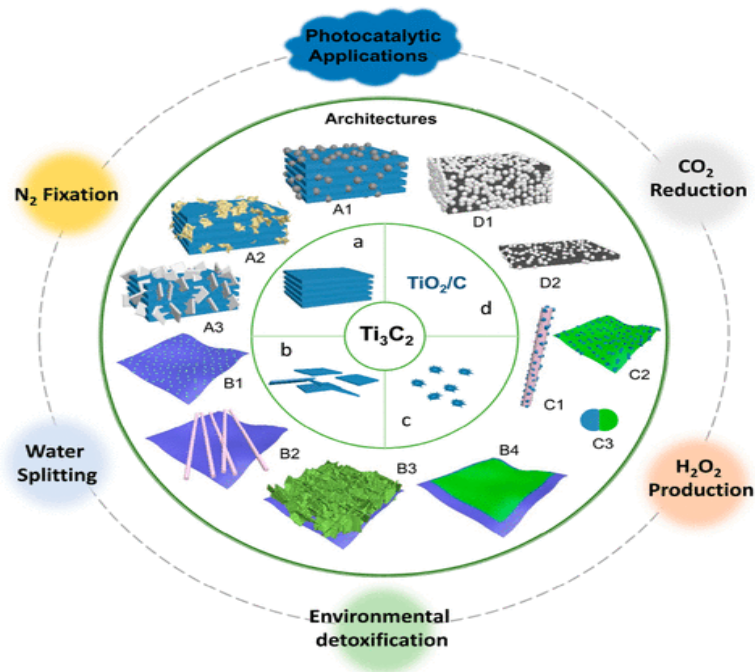


Figure 12: Applications of MXenes as Photocatalytic Agents [44].

2.3.5 Applications of MXenes as Antibacterial Agents

Antibacterial infections need to be addressed in various contexts. The primary applications of MXene-based antibacterial polymers have been explored in solar-powered water purification devices, wound dressings, and membranes for water purification.

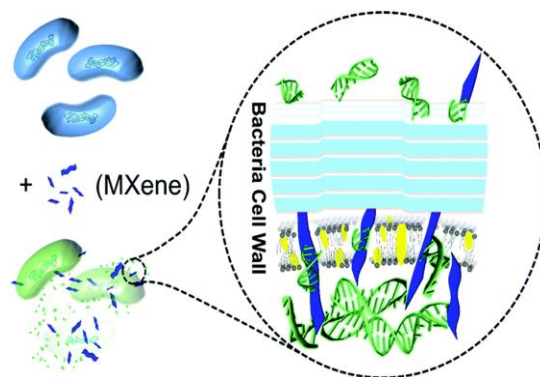


Figure 13: Antibacterial Activity of MXenes [45].

2.4 Literature Survey of Photocatalytic Activity of MXene and MXene Based Nanocomposites

2.4.1 Review of Problem

Increasing global industrialization has adversely affected the availability of potable water by introducing harmful substances such as organic dyes and pharmaceutical waste i.e. antibiotics into water sources.

In **2014**, MXene was initially employed as a photocatalyst. Since then, numerous papers have been published on its use in degrading toxic contaminants from air and water. Several factors contribute to its effectiveness as a photocatalyst, including the presence of functional groups created through wet chemical etching[46],[47].

In **2018**, Liu et al studied and reported the complete degradation of ciprofloxacin antibiotic in 150 minutes with 10mg g-C₃N₄/Ti₃C₂ MXene as photocatalyst in 50ml of ciprofloxacin solution(20mgL⁻¹). The g-C₃N₄ nanosheets were prepared in muffle furnace and g-C₃N₄/Ti₃C₂ MXene based composite was synthesized via evaporation induced self-assembly method[48],[49].

In **2021**, Thirumal et al reported the photocatalytic degradation of 50ml of 2ppm Methylene dye using visible light, Ti₃AlC₂ MAX and Ti₃C₂ MXene as photocatalyst. The dye showed poor degradation of 23% under visible light irradiation. It showed 40% degradation using MAX and 50% degradation using MXene as photocatalysts respectively[50].

In **2022**, Park et al reported the synthesis of cobalt-doped ZnTiO₃/Ti₃C₂ MXene based nano-hybrids as photocatalyst via self-assembly method. It had been observed that tetracycline antibiotic was degraded up to 76.3% by using 500mg/L of this photocatalyst under visible light irradiation conditions[51].

In **2023**, Chen et al reported that BiOCl/Ti₃C₂Tx MXene heterojunction was synthesized via electrostatic self-assembly. With 0.25% MXene loading, it can photodegrade up to 90% of CIP in

30 minutes. The Schottky barrier formed between BiOCl and Ti_3C_2Tx MXene reduces electron-hole recombination, enhancing photoactivity[52].

In **2024**, Shilin Li et al reported the synthesized of $ZnO@Nb_2CT_x$ MXene@carbon nitride nanosheets as photocatalyst. The $ZnO@Nb_2C$ was prepared by hydrothermal method and $ZnO@Nb_2CT_x$ MXene@carbon nitride nanosheets was synthesized via electrostatic self-assembly method. It had been observed that $500mgL^{-1}$ photocatalyst showed 98.2% degradation of enrofloxacin antibiotic solution($10mgL^{-1}$)[53].

Chapter 3

Apparatus and Experimental Measurements

This chapter describes the apparatus and experimental measurements and parameters used to synthesize the Mxene and its composites, as well as the testing procedures of photocatalysts to degrade antibiotics. Afterwards, all necessary characterization techniques will be described here. XRD, SEM, EDX, RAMAN, FTIR, UV VIS Spectroscopy and PL(Photoluminescence) spectra etc. are used to analyze the structural elements and photocatalytic properties of materials will be covered here.

3.1 Chemicals

The chemicals listed below in table 1.1 are used for the synthesis of Mxene from MAX and its composites.

Chemical	Purity	Source
Hydrofluoric Acid (HF)	48%	Sigma
Nitric Acid (HNO ₃)		Sigma
Deionized Water DI	99.8%	Sigma
Ethanol	99.8%	Sigma
Acetone	99.8%	Sigma
CTAB (Cetyltrimethylammonium Bromide)	99%	Sigma
NaBH ₄ (Sodium borohydride)		
Silver Nitrate (AgNO ₃)	99.8%	Sigma
MAX (Nb ₂ AlC)		

3.2 Apparatus Description

The given list is of the commonly used apparatus throughout the period of experimental and synthesis process.

- Weight balance
- Hot plate
- Teflon beakers

- Glass beakers
- Spatula
- Heavy duty gloves
- Butter paper
- Aluminum foil
- Vacuum drying oven
- Droppers
- Vials
- Petri dish
- Vacuum desiccator
- Fume hood
- Respirators
- 0.22um pore size filter papers
- Centrifuge machine
- Thermometer
- Vacuum filtration assembly
- Falcon tubes
- Tweezers
- Magnetic stirrers
- Water bath sonicator
- Halogen lamp

3.2.1 Digital Weight Balance

Digital weight balance measures the weight and mass of objects and sample materials with high accuracy and precision. We have a digital weight balance in our lab for measuring purposes with least count of 0.1 mg. A typical digital weight balance with a protective glass surrounding it for safe laboratory environment is given below in fig 14.



Figure 14: Digital Weight Balance.

3.2.2 Hot Plate

The hot plate is a laboratory instrument used for heating and stirring the liquids and solutions simultaneously. Typically, a filament element is used to heat the metallic or ceramic surface of hot plate. Additionally, it has the magnetic stirring system to mix solutions properly with the help of magnetic bar stirrer. The typical lab hot plate is given below.



Figure 15: Hot Plate.

3.2.3 Fume Hood

A fume hood is a vital safety enclosed workplace in lab where hazardous fumes, vapors and dusts are generated during chemical reactions, experiments and processes. It has a moveable glass or acrylic door or window and is connected to the ventilation system that exhausts toxic

gases and vapors in the outer environment. While dealing with hydrofluoric acid, HF, careful precautions should be practiced, including the usage of heavy-duty gloves, respirators, protective face shield and goggles. Not only with HF, while dealing with other toxic chemicals and acids, fume hood plays a very important role.



Figure 16: Fume Hood [54].

3.2.4 Centrifuge Machine

The HERMLE 50 ml centrifuge machine works by spinning samples at high speed, creating a centrifuge force that pushes the heavier particles outward, separating them from the lighter one based on their densities. The solid particles with high density settle at the bottom of the tube, forming a clay, while the supernatant with few lighter particles remains above. This machine is mostly used for separating precipitates from solutions and purifying various compounds. This machine works with the variation of time from a few seconds to several hour with the maximum speed limit up to 11,000 rpm.

3.2.5 Vacuum Filtration Assembly

A vacuum filtration assembly is a setup used in labs to filter or separate the solids from liquids quickly and efficiently by applying vacuum pressure. It contains essential components like filter funnel, filter flask, filter paper or membrane, rubber or silicon stopper and a vacuum source.

3.2.6 Vacuum Drying Oven

In lab settings, vacuum drying ovens are favored for drying the prepared wet samples under low oxygen environment. As wet or humid samples are more prone to be oxidized easily. In an open environment, an oxidative layer or upper layer of wet material or sample is oxidized when it is heated. So, this process is less likely to happen under the controlled environment of oven while heating. Its temperature can be adjusted up to 400 °C using a temperature controller and it operates in a pressure range of 10⁻³ torr.



Figure 17: Vacuum Drying Oven.

3.2.7 Water Bath Sonicator

A water bath sonicator is a crucial tool in labs for preparing samples and creating homogenous solutions. It works by emitting high frequency sound waves in a container filled with liquid containing a sample and a solvent. It creates cavities inside liquid induces small bubbles that collapse with force, effectively cleaning surfaces or dispersing materials using ultra sound waves. It plays an important role to homogenize the solutions especially. So, the illustration of this valuable tool is given below.

3.2.8 Halogen Lamp

The halogen lamp is a type of incandescent lamp made up of filament tungsten and contains small amount of a halogen gas such as iodine or bromine. In laboratories, halogen lamp serves for many purposes such as heating source, light source and for photocatalysis. In our lab, Halogen lamp plays an important role in photocatalytic processes, including the photocatalytic

degradation of organic pollutants. In these processes, the halogen lamp serves as the light source that activates photocatalysts such as titanium dioxide (TiO_2) or MXene-based materials. When exposed to light, these photocatalysts generate reactive oxygen species (ROS) that can break down organic pollutants in water or air.

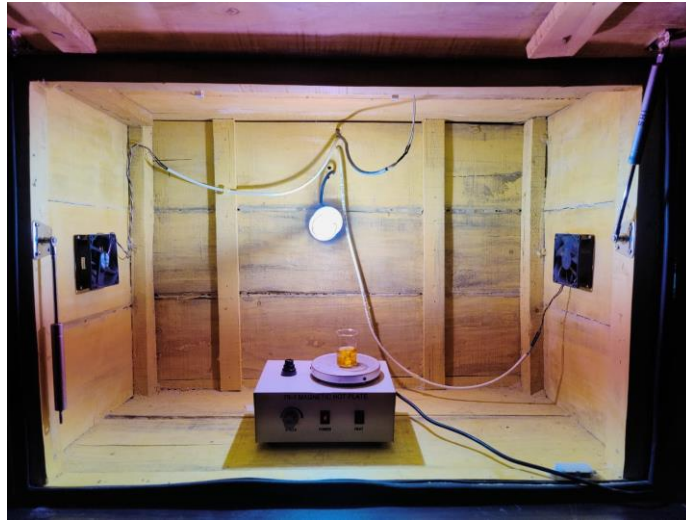


Figure 18: Halogen Lamp.

3.3 Characterization Techniques

We can ensure the quality of our samples and materials by using qualitative and quantitative analysis. By assessing morphology, structural properties, optical characteristics and electrochemical behavior, we can determine the success of the synthesis process. The main characterization techniques that we use in our study are given below.

- X-Ray Diffraction (XRD)
- Scanning Electron Microscope (SEM)
- Energy Dispersive X-ray Spectroscopy (EDX)
- Raman Spectroscopy
- Fourier Transform Infrared spectroscopy (FTIR)
- Ultraviolet Visible spectroscopy (UV)
- Photoluminescence spectra (PL)

3.3.1 X-Ray Diffraction (XRD)

X-ray diffraction is a powerful, non-destructive analytical technique used to study the atomic and molecular structure of material. When X-rays with specific wavelength are directed at a crystalline material, they are diffracted in different directions by interacting with the electronic cloud surrounding the atoms in crystal lattice. As X-rays scatter off the crystal lattice, they create a specific pattern consists of constructive and destructive interference of X-rays, resulting in peaks and troughs of intensity. The samples for XRD analysis are mostly in powder or thin film to ensure the orientation of crystal planes. The diffraction pattern satisfies the Bragg's Law which relates the angles of incidence of X-rays to the d- spacing between the crystalline planes and wavelength of X-rays.

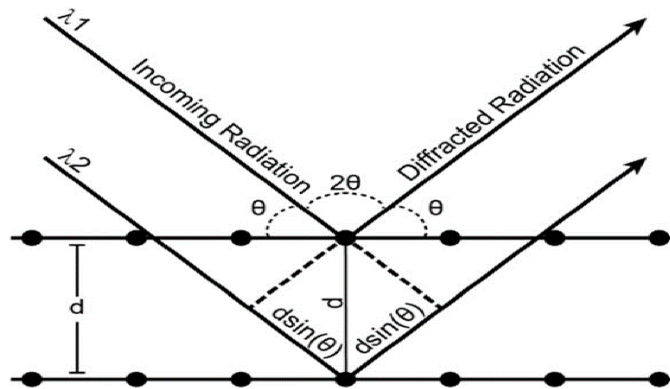


Figure 19: Phenomenon of Bragg's Law Conditions [55].

W. L. Bragg and W. H. Bragg described how atoms in a crystal align regularly, allowing X-rays to interact with them. The X-rays have fixed wavelength comparable to the d-spacing between the crystal lattice planes and strike the crystal at specific angle. Upon scattering from the atomic planes in the lattice, X-rays exit the crystal at the same angle as they entered. This results in a path length traveled by the rays, with differences in this path length being integer multiples of the X-ray wavelength. The interference pattern is then recorded as counts per second against the angle 2θ . Bragg formulated a law, known as Bragg's law, which relates the wavelength of the incident ray to the incident angle θ and the interlayer spacing d , expressed in Equation 1.

$$n\lambda = 2d\sin\theta \quad (1)$$

here;

n integer representing order of reflection

d represents distance between diffraction planes

θ represents incident angle

λ is incident ray wavelength

The powdered XRD analysis is very beneficial to determine the crystal structure, phase composition, lattice parameters, and orientation of crystalline domains within the material.

3.3.2 Scanning Electron Microscope

SEM is a versatile and powerful tool in material sciences plays crucial role in offering the detailed imaging, surface analysis and elemental analysis at nanoscale resolution. Its functional principle is electron-matter interactions, providing detailed view of sample's surface at high resolution. SEM uses a fine beam of electrons to scan the surface of material

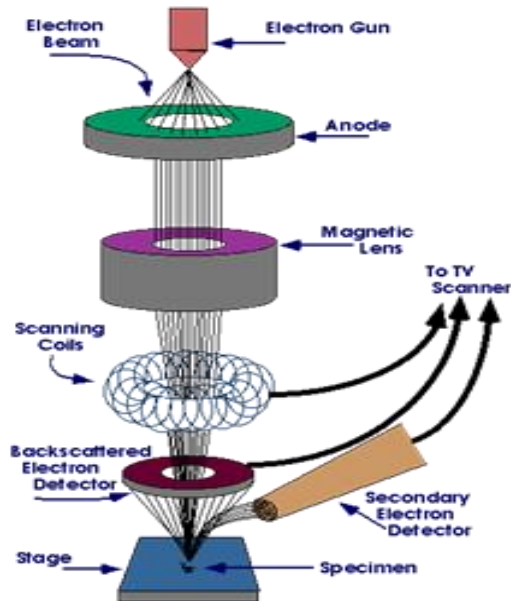


Figure 20: Schematic diagram of Scanning Electron Microscope[56].

. Various signals such as scattered electrons (SE) and backscattered electrons (BSE) are emitted and utilized for imaging when electron beam interacts with sample. In SEM, SE are

the electrons emitted from the sample's surface when electron beam interacts with it, giving the detail of texture and structure. While, on the other hand, BSE are the electrons reflect off the atoms of surface and provide description about the elemental composition and density. So, in SEM, they work together to give the complete picture of surface analysis and materials density. In industrial realms, SEM plays a crucial and beneficial role for assessing the defects and exploring the topography, composition and surface features of diverse materials.

3.3.3 Energy Dispersive X-ray Spectroscopy (EDX)

Energy Dispersive X-ray Spectroscopy is a technique commonly used alongside SEM to analyze the chemical composition of sample. In the EDX procedure, when a high energy electron beam by SEM is bombarded on to the sample, it emits characteristic X-Rays due to the interaction between high energy electrons and atoms with in sample. These emitted X-rays have distinct energies that are specific to the elements present in the sample. An EDX detector attached to the SEM collects and measures the energy of these X-rays. This measurement allows for the identification and quantification of elements in the sample. Moreover, SEM-EDS are more beneficial due to elemental mapping allows the visualization of elemental composition across the sample's surface and provides the insights of elemental arrangement in the sample.

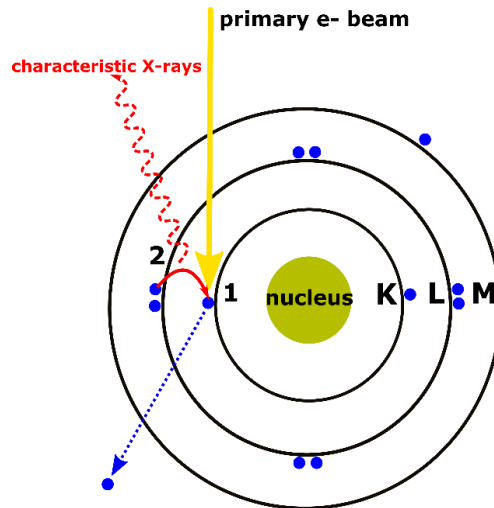


Figure 21: Generation of X-Rays[57].

3.3.4 Raman Spectroscopy

A highly powerful, non-destructive analytical method that allows to study the vibrational, rotational and other low frequency modes of molecules in samples is known as Raman spectroscopy. It provides information regarding chemical structure, phase, crystallinity and molecular interactions. When a monochromatic light, mostly, laser beam falls on to the sample, most of the photons undergo elastic scattering known as Rayleigh scattering where the 90% intensity and wavelength remain same as of the laser beam. Remaining small fraction of photons undergo inelastic scattering named as Raman scattering, during which they interact with the sample molecules and loss or gain energy. The chemical bonds interact with light and gives the required information on the screen. The scattered light containing both Rayleigh and Raman scattered photons are collected and passed through a spectrometer. The spectrometer disperses the light into its component wavelengths and measures the intensity of each wavelength. This process generates a Raman spectrum, which is a graph showing intensity (y-axis) versus Raman shift (x-axis). So, the “molecular fingerprint” of the target material is obtained as a result of Raman analysis. The important components of Raman spectroscopy are given below.

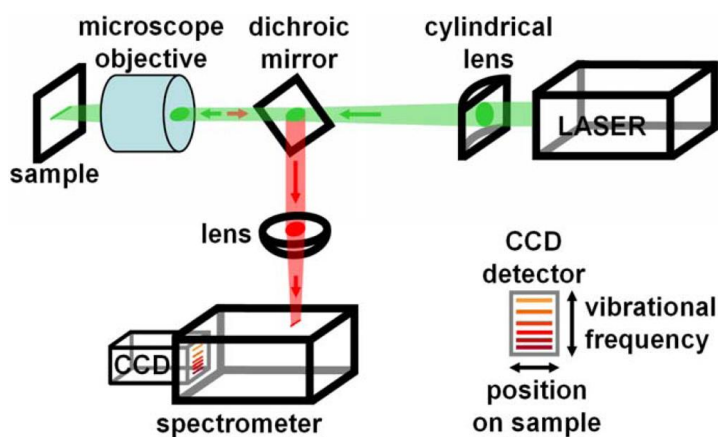


Figure 22: Raman spectroscopy schematic [58].

3.3.5 Fourier Transform Infrared Spectroscopy (FTIR)

Fourier transform infrared spectroscopy is a crucial technique used for the detection and identification of functional and chemical groups in the sample. The sample is exposed to

infrared electromagnetic radiations ranging from 10000 cm^{-1} to 100 cm^{-1} and 4000 cm^{-1} to 400 cm^{-1} . The sample undergoes vibrational transitions when it absorbs these infrared radiations which are then studied in spectroscopic analysis. A standard FTIR contains several key components, including a source radiation, detector, interferometer, a sample compartment, an amplifier, an analog to digital converter (A/D converter) and a computer. The radiation emitted from the source passes through the sample via interferometer and detected by detector.

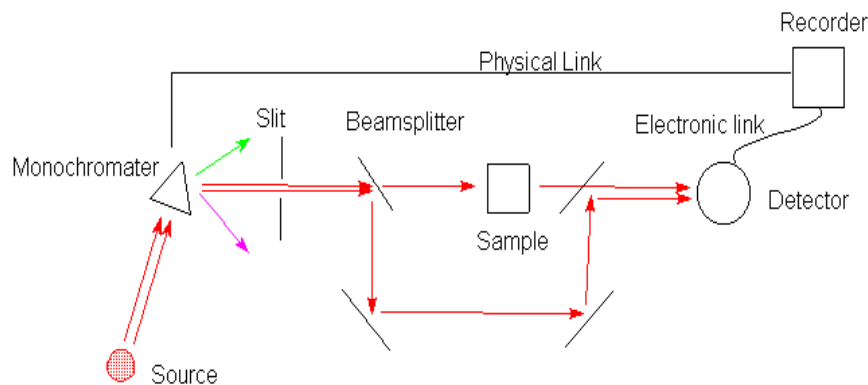


Figure 23: Working of FTIR spectrometer [59].

The signal is amplified and converted into digital format by an amplifier and analog to digital converter respectively. Then, the digital signal is processed in the computer using Fourier Transform.

The principle underlying FTIR is based on Michelson interferometer. It operates by splitting the single light beam in two parts and then altering their parts differently and recombines them within the interferometer. The detector calculates the intensity difference between these two photons based on their paths.

3.3.6 Photoluminescence (PL) Spectra

Photoluminescence spectra is a powerful and non-destructive technique to assess the recombination rate of charge carriers in nanostructures especially in semiconductor materials with direct band gap. This characterization only needs very small amount of sample. When sample is exposed to light, electron-hole pairs generate that recombine over a short period. This technique observes this recombination, generates PL curves that indicate the extent of

recombination. These PL curves can be directly correlated to photocatalytic measurements, as they share a direct dependence on the recombination rate of charge carriers.

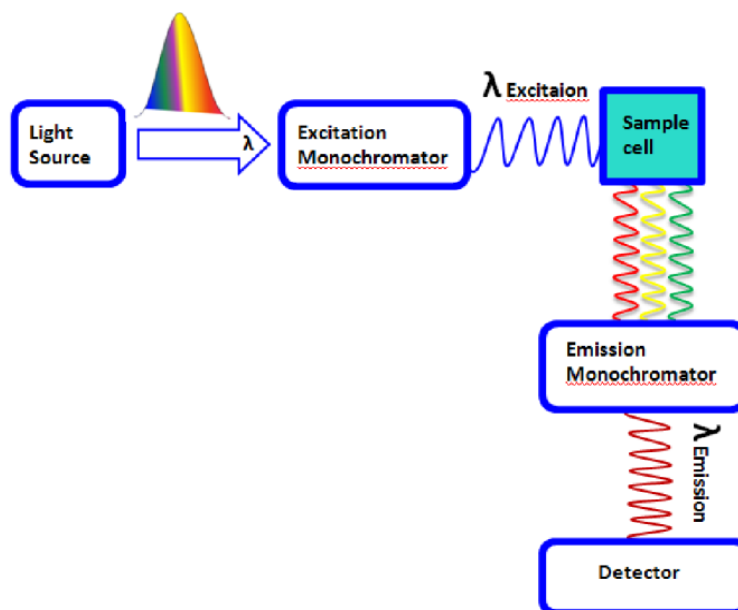


Figure 24: Working of Photoluminescence (PL) Spectra [60].

3.3.7 Ultraviolet-Visible Spectroscopy

Ultraviolet-Visible spectroscopy is a powerful technique, particularly in the ultraviolet and visible ranges, used to analyze how molecules transmit, reflect and absorb light. The basic principle underlying here is the law of Beer Lambert's and according to this law, the absorption of light is directly proportion to the concentration of molecules in the sample in the cuvettes and path length of cuvettes. In this spectroscopy, the fine beam of light with known intensity is absorbed by specimen, excites and de-excites atoms and measures the decrease in the intensity. The concentration or number of molecules come into the path is related to intensity. In UV-VIS spectroscopy, typically two cuvettes, one with reference sample and other with the test sample are used. Firstly, reference sample is tested with ultraviolet-visible light and the amount of transmitted light is noted. Then test sample is exposed to light, some light is absorbed and some is reflected. The electrons in the molecules of test sample jump from lower to higher orbit in bad structure and the intensity of light at that given wavelength is detected by detector.

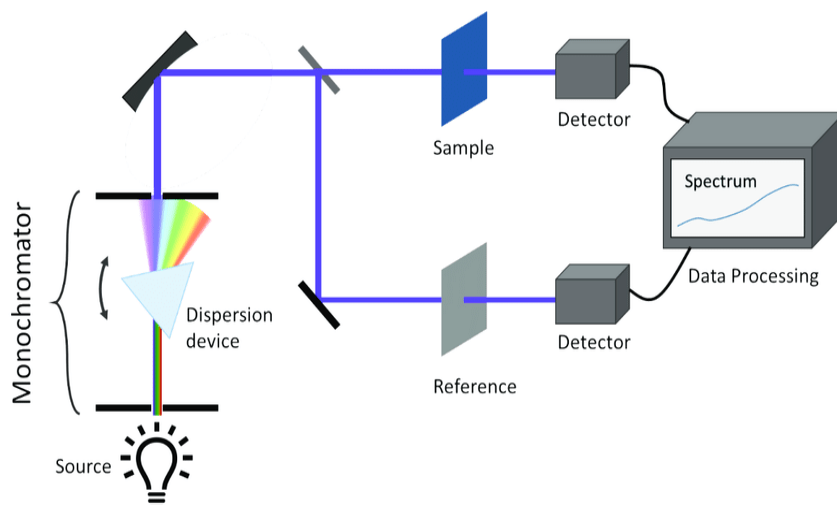


Figure 25: Double Beam Spectrophotometer [61].

3.3.8 Photocatalytic Measurements

The photocatalytic properties of as prepared sample or photocatalyst are analyzed using UV-VIS spectroscopy. The antibiotic contaminated solution is prepared in DI water by dissolving 10 mg antibiotic per liter DI. For experiment, 3mg, 6mg, 10mg, 15mg, and 30mg of prepared catalyst is added in the 30ml of as prepared antibiotic solution in the beaker. The solution is illuminated by using 400 W halogen lamp. Prior to the visible light irradiation, the solution and photocatalyst are stirred under dark conditions for 60 minutes to achieve the adsorption/desorption equilibrium. During irradiation, 2ml solution is removed after every 30 minutes interval and separated by centrifuge at 10000 rpm. Then the supernatant is analyzed by measuring the maximum absorbance using double beam UV VIS spectrophotometer.

Chapter 4

Synthesis and Result Analysis

4.1 Synthesis Procedure

In this section, we will cover the synthesis of the materials prepared in this work. First, we will discuss the etching parameters of Nb₂AlC MAX. Following this, we will discuss the delamination of MXene using two different solvents: TMAOH and isopropylamine. Then, we will discuss the synthesis of the Nb₂C and silver composite and its application in the field of photocatalytic degradation of antibiotics and dyes.

4.1.1 Etching of Nb₂AlC MAX

To synthesize Nb₂C, the MAX phase Nb₂AlC (with a mesh size of 200) was treated with HF for 96 hours at a specific temperature in a Teflon beaker placed in silicon oil bath. In 20 ml of 48-50% concentrated HF, 1 g of Nb₂AlC was slowly added to avoid localized heating.

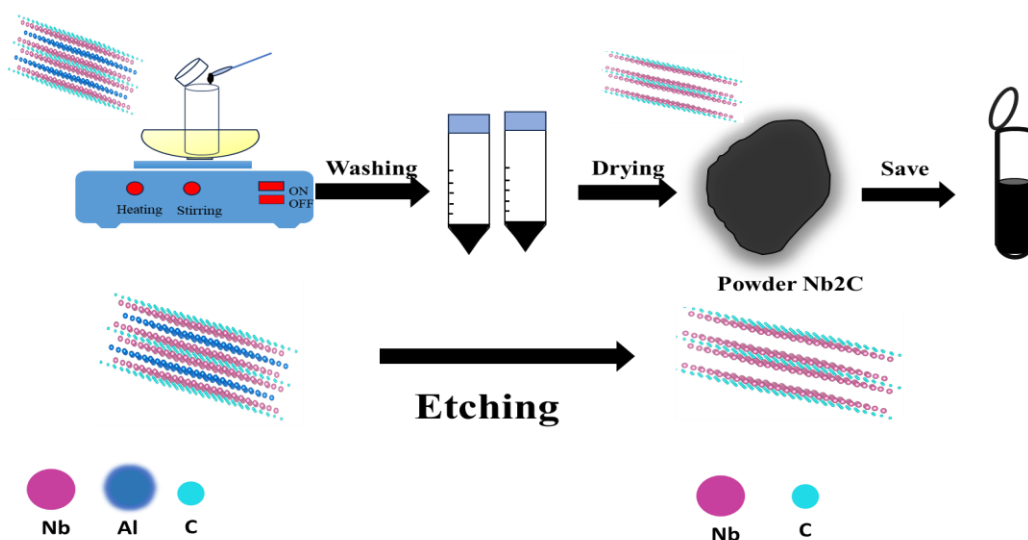


Figure 26: Synthesis of Nb₂CT_x MXene.

The solution was kept at 50-60°C for 96 hours, stirring at 450 rpm. The etched powder was then washed several times with deionized water until the pH exceeded 6. The powder was subsequently

dried by filtration assembly. The dried powder on filter paper was then placed in a vacuum oven at 25-35°C for 24 hours. Finally, the dried powder was kept in an Eppendorf tube in a vacuum desiccator.

4.1.2 Delamination of Nb₂C MXene with Isopropyl Amin (i-PrA)

To obtain delaminated Nb₂C, multilayered Nb₂CTx was first intercalated with isopropylamine (i-PrA, 99.5% Sigma-Aldrich). 1g of MXene was immersed in 10 mL of an i-PrA aqueous solution, diluted with deionized water in a 1:4 ratio of i-PrA: H₂O. This mixture was stirred at room temperature for 18 hours using a magnetic stirrer. The suspension was then centrifuged for ten minutes at 8000 rpm and decanted. The remaining intercalated MXene powder was suspended in 45 to 50 mL of deionized water and sonicated for one hour, with the centrifuge tube covered with parafilm. After sonication, the suspension was centrifuged for one hour at 3500 rpm to separate the single-layer MXene, which remained in suspension, from the multilayer MXene, which settled. The delaminated MXene was separated from the multilayered MXene, dried by filtration assembly and then placed in vacuum drying oven to dry completely[62].

4.1.3 Synthesis of Silver Nanoparticles

Ag NPs were synthesized using a simple electrostatic self-assembly method through the chemical reduction of AgNO₃ salt. In brief, at room temperature, 50 mL of 9.0 mM aqueous solution containing silver nitrate(75mg) was prepared under stirring. Then 50mg CTAB was added (acts as surfactant and gives positive charge to the silver). The mixture was then stirred for 30 minutes to achieve homogeneity. 10ml of 8mM refrigerated cool sodium borohydride (3.1mg) was added dropwise into the prepared mixture solution. Immediately, the solution turned into bright yellow indicating the formation of silver nanoparticles (Ag NPs). Left solution under stirring for 1 hour[63].

4.1.4 Synthesis of Nb₂C and Ag-NPs Composite

To synthesize Nb₂C/Ag NP composites, we use 100mg MXene and 75mg, 50mg and 25mg AgNO₃ salt. We make three composites in the ratios of Nb₂C: Ag NPs are 1:0.75, 1:0.5, 1:0.25. An aqueous solution of Ag NPs (0.5mg/ml) and a colloidal solution of Nb₂C(1mg/ml) Mxene was mixed and sonicated for 30 minutes and then stirred for 30 minutes at 35-40 °C to achieve homogenous

suspension and vacuum filtered to get the Nb₂C/Ag NPs composite. The filtered material was then dried in vacuum oven at 60 degrees for overnight[63].

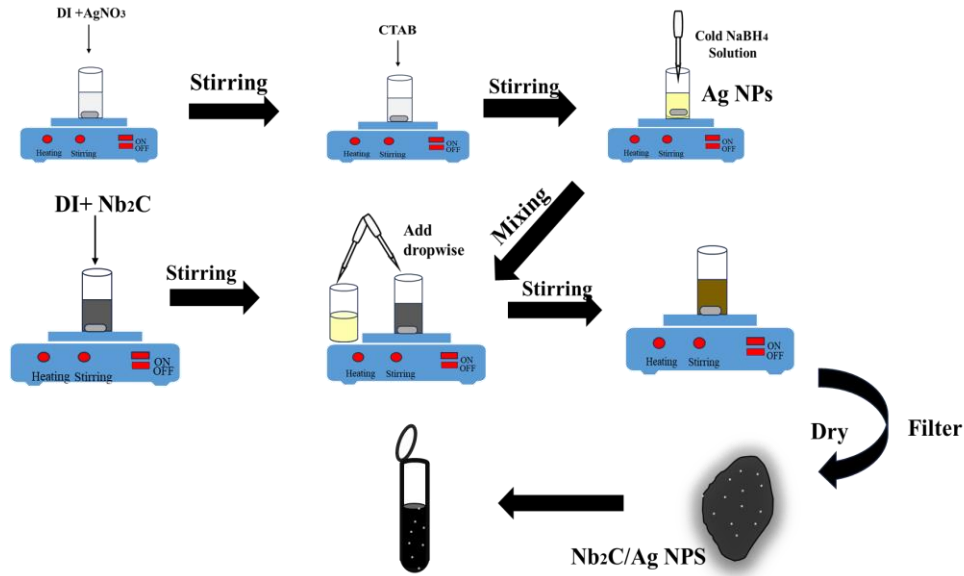


Figure 27: Synthesis of Nb₂CTxMXene/Ag NPs Composite.

4.2 XRD Analysis

In this section, we will discuss about the XRD analysis of Nb₂AlC MAX, Nb₂C MXene, delamination of Nb₂C MXene with isopropyl amine. Then we will discuss about the XRD analysis of Nb₂C MXene composite with silver nanoparticles.

4.2.1 XRD Analysis of etching of Nb₂AlC

X-ray diffraction (XRD) analysis provides detailed information about the material's structure. After HF treatment, the peak observed at (002) in the MAX phase becomes broadened and shifts towards a lower angle. This indicates the removal of the Al layer from the MAX phase, resulting in an increased d-spacing. The (103) peak signifies the presence of aluminum, while the other peaks correspond to intermetallic peaks.

As we have seen from the XRD plots in fig 28, the (002) peak is shifted at the lower angle in case of MXene. Firstly, it is at 12.65° then after the HF treatment, it is shifted at 7.9° so its d- spacing increases from 6.99(Å) to 11.18(Å) and c- lattice parameter increases from 13.98(Å) to 22.36(Å).

The unetched MAX is also present as seen from (103) peak at 38.05° which is of Aluminum.

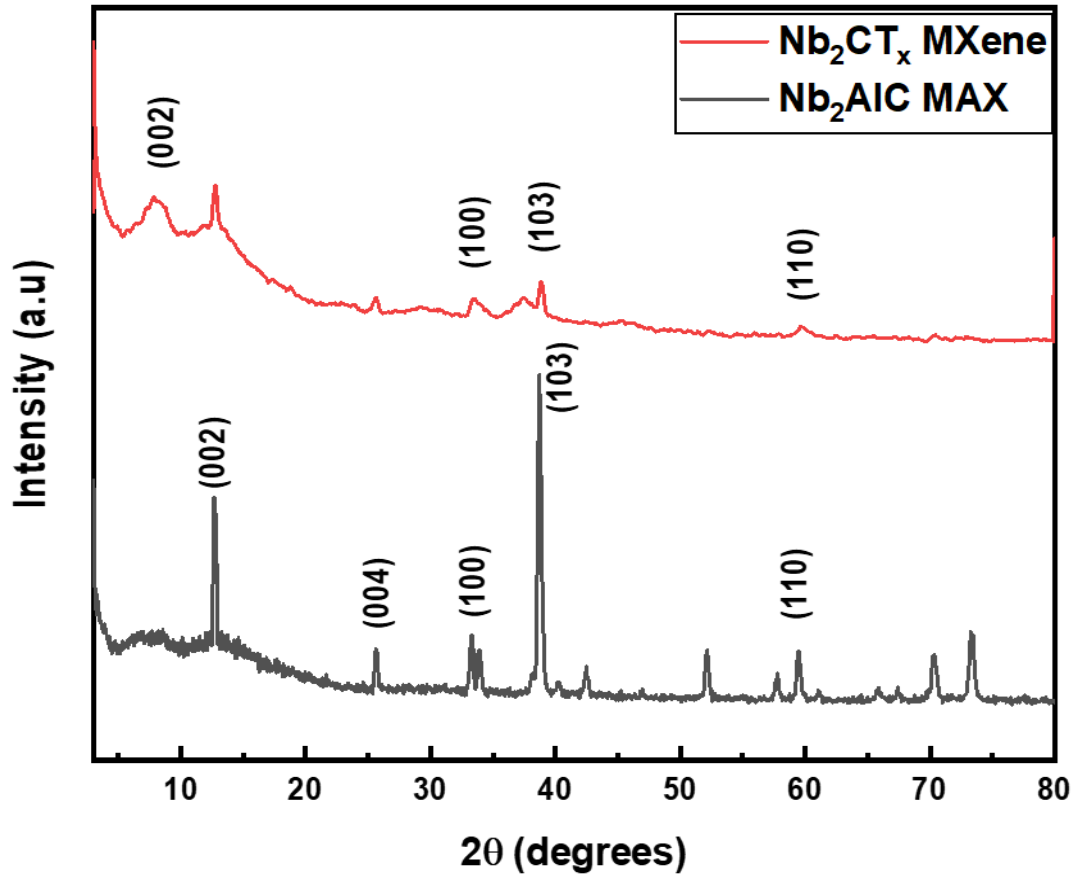


Figure 28: XRD Analysis of MAX and MXene.

4.2.2 XRD Analysis of delaminated MXene using isopropyl amine

The delamination of Nb₂C from i-prA has stronger intercalation ability and superior etching properties. As we can see from the XRD plots that there is a (002) peak shifting towards lower angle from 7.9° for MXene to 6.75° for delaminated MXene. The corresponding d-spacing increases from 11.04(Å) to 13.09(Å) and c-lattice parameters also increases from 22.36(Å) to 26.17(Å).

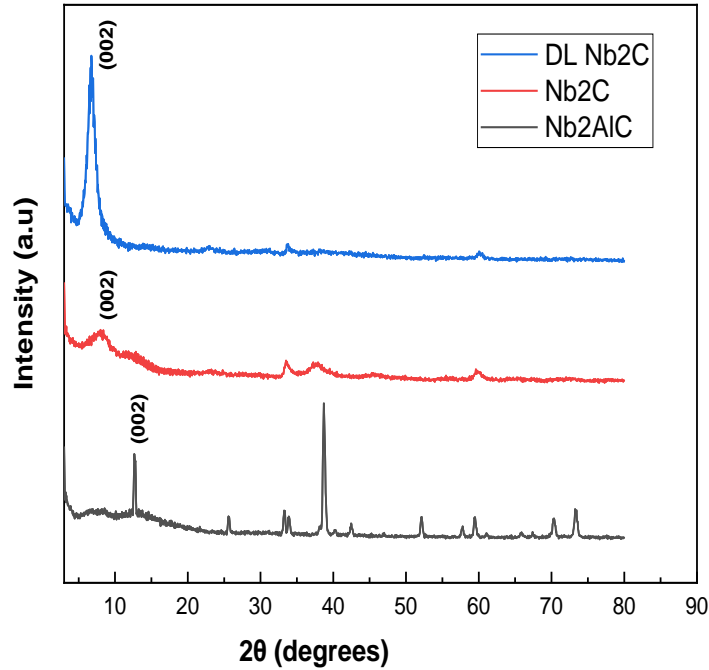


Figure 29: XRD analysis of MAX, MXene and delaminated MXene.

4.2.3 XRD Analysis of Nb₂C/Ag-NPs Composite

XRD analysis shows successful composition of Nb₂C- Ag NPs, as the peaks at 38°(111), 44° (200), 64° (220) and at 77° (311) shows the presence of Ag nanoparticles and the (002) shifts from 7.9° to 8.2° which shows the presence of Ag nanoparticles between MXene layers.

The corresponding d- spacing also decreases from 11.04(Å) to 10.51(Å) and c-lattice parameters also decreases from 22.08(Å) to 21.03(Å) due to intercalation of Ag NPs among the sheets of MXene. The unetched MAX is also present as seen from (002) peak at 12.65° and (103) peak at 38.05° which is of aluminum.

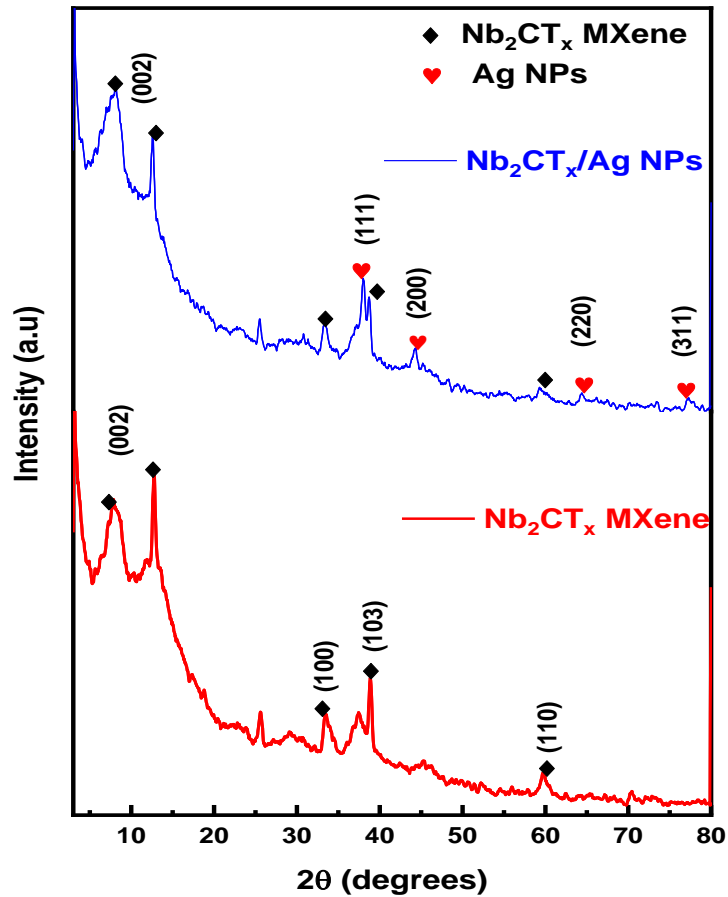


Figure 30: XRD Analysis of MXene and Mxene/Ag NPs composite.

4.3 Scanning Electron Microscope (SEM)

This section consists of SEM images of Nb₂AlC MAX, MXene and the composite of MXene and silver nanoparticles.

4.3.1 SEM Images of MAX and MXene

Figure 31(a) displays the MAX image of Nb₂AlC, highlighting its lump-like morphology. This image provides insight into the surface topography and texture of the MAX phases and also reveal the grain size. After etching Nb₂AlC, fig 31 (b) and (c) depict the layered structure of MXene. This is a result of the removal of the aluminum layer, which creates separation between the MXene sheets, thereby confirming the etching process. Additionally, surface impurities can be observed on the MXene sheets, indicating the presence of aluminum fluoride and unreacted MAX phases. Some impurities also arise from the functional groups that attach to the MXene surface after etching.

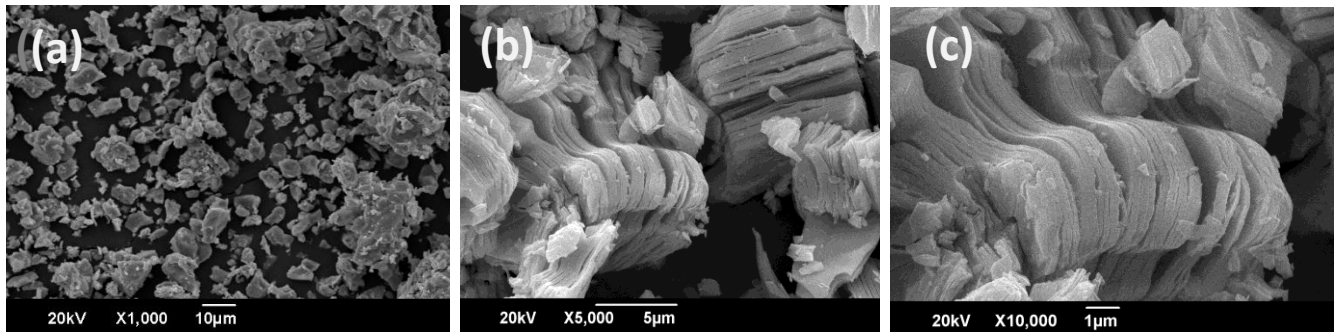


Figure 31: SEM Images of (a) Nb₂AlC MAX at 10μm, (b) and (c) Pristine Nb₂CT_x MXene at 5μm and 1μm respectively.

4.3.2 SEM Images of Nb₂C-Ag NPs composite

The SEM images of Nb₂C-Ag NPs composite are shown below which represents the successful intercalation of Ag nanoparticles on MXene's surface and sheets.

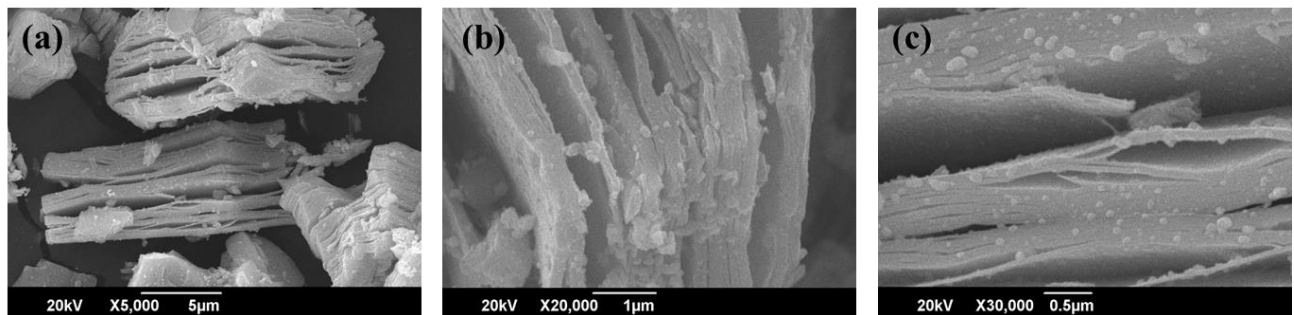


Figure 32: SEM Images of (a), (b) and (c) Nb₂CT_x/Ag NPs composite at 5μm, 1μm and 0.5μm respectively.

4.4 Energy Dispersive X-Ray Spectroscopy (EDX)

EDX provides the elemental mapping or weight, or atomic mass of elements present in the material. In this section, the elemental mapping of MXene and composite are discussed in detail.

4.4.1 EDX of MXene

As we can see in fig 33(a), there are Nb, O, C, F and very low quantity of Al which shows the successful etching of Nb₂C MXene from Nb₂AlC MAX phase. There is also a peak of Fluorine which are terminations that were attached to the Mxene surface during etching and there is an

increase in the peak of Oxygen which is due to the terminations that were attached during washing process of MXene. So, this confirms the formation of MXene.

4.4.2 EDX of Nb₂C-Ag NPs

The EDX analysis of Nb₂C-Ag NPs composite is shown in fig 33(b). The peaks represent the quantity or weight % of an element in the material.

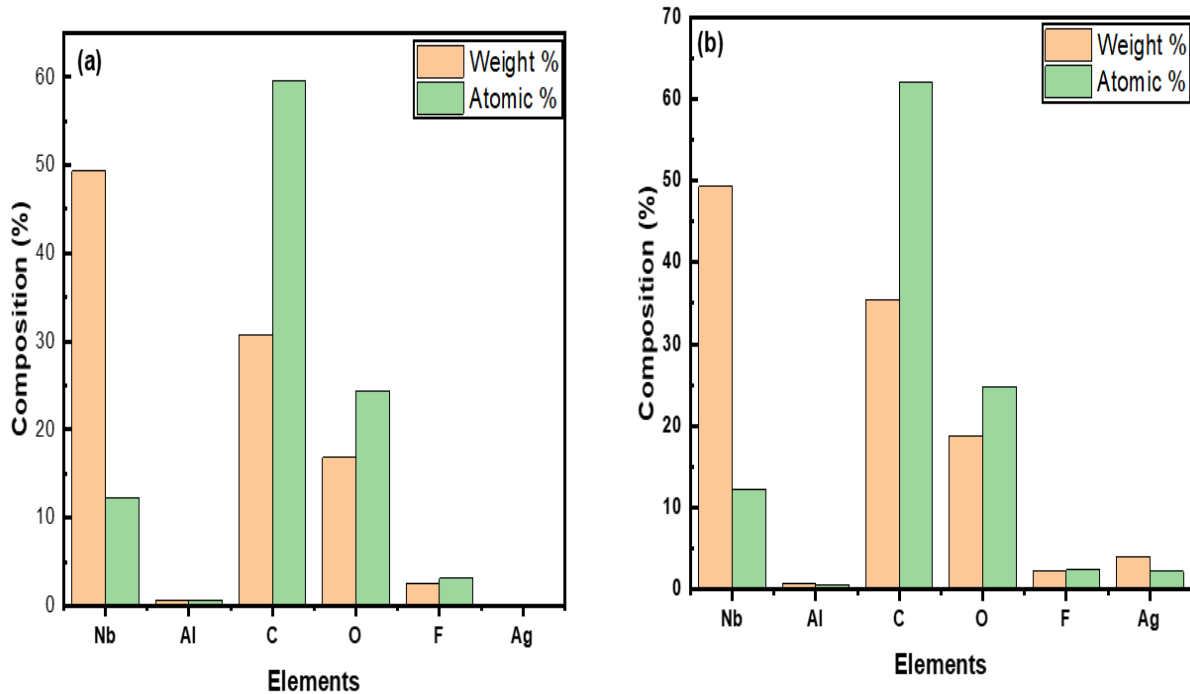


Figure 33: (a)EDX analysis of MXene and (b) MXene/Ag NPs composite.

There are carbon C, oxygen O, a small amount of fluorine F, and a small amount of aluminum Al due to HF treatment and remaining unetched aluminum. There is also a peak of silver which shows the successful intercalation of silver in MXene.

In both, the morphology is not affected where the elemental content present in Nb₂C- Ag NPs as prepared material is displayed in fig 33(a). which was performed to confirm the presence of Ag NPs in Nb₂C MXene. Fig 33 shows the EDX of Nb₂C MXene and Nb₂C-Ag NPs composite.

4.5 Raman Spectroscopy

In fig 34(a), the first peak in the Raman spectrum of MAX phase at 131 cm⁻¹ shifts slightly towards a higher frequency in MXene, indicating either the removal of aluminum or increased interlayer

spacing. The subsequent peaks at 257 cm^{-1} and 410 cm^{-1} are associated with the in-plane (E_g) vibrations of Nb atoms and the surface groups attached to them. The peak at 627 cm^{-1} corresponds to the active carbon vibration modes (A_{1g}) in MXene, specifically related to $\text{Nb}_2\text{CO}(\text{OH})_2$, providing further evidence of etching through the presence of $-\text{O}$, $-\text{OH}$, and $-\text{F}$ surface terminations[64].

For Nb_2C , the characteristic peaks appear at 125 cm^{-1} , 257 cm^{-1} , and 410 cm^{-1} , representing the in-plane E_g vibrations of Nb atoms and their associated surface groups. The peak at 627 cm^{-1} , corresponding to the A_{1g} modes of MXene, further confirms these features. When Nb_2C is combined with Ag, no significant peak shifts are observed, suggesting that the Nb_2C retains its high quality after composite formation, with Ag particles responsible for the enhanced peak intensity. Notably, since Ag itself does not produce peaks in Raman spectroscopy, the enhancement is attributed to the presence of Ag particles within the Nb_2C structure[65].

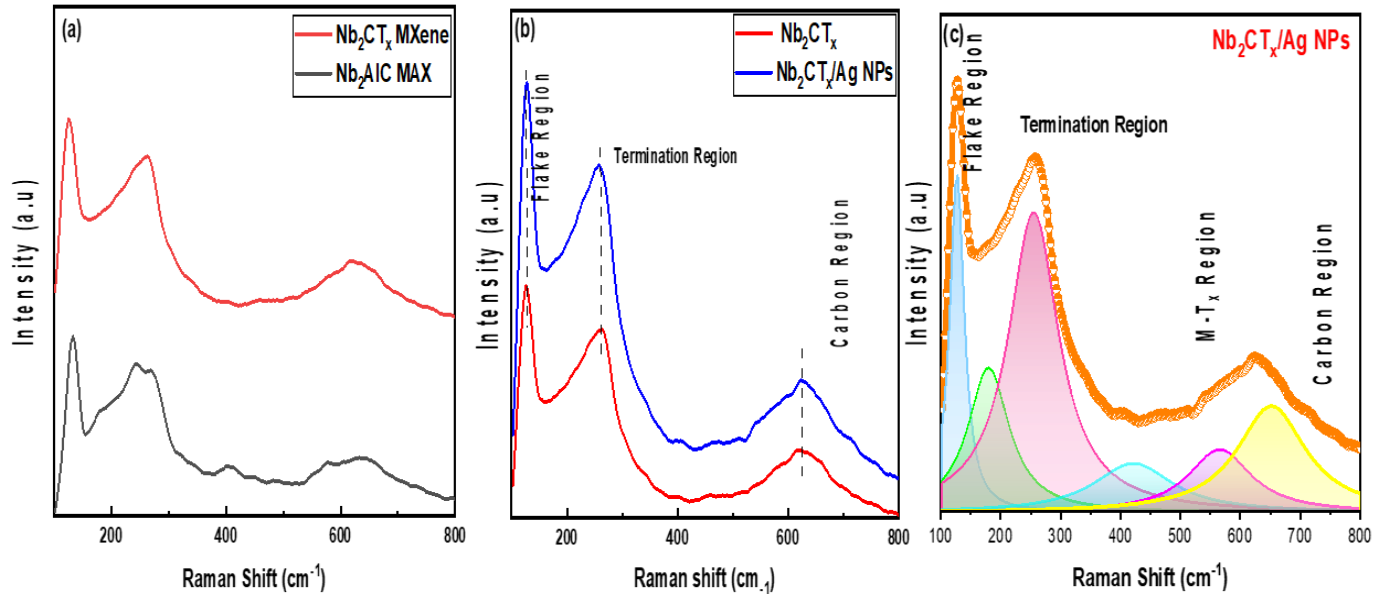


Figure 34: (a) Raman spectra of MAX and MXene (b)MXene and Composite (c) deconvoluted spectra of $\text{Nb}_2\text{CT}_x/\text{Ag NPs}$ composite.

Fig 34(c) illustrates the deconvoluted Raman spectra of the $\text{Nb}_2\text{C}/\text{Ag NPs}$ nanocomposite, where for deconvoluted and fitted graph, Lorentz function had been used. The prominent peak at 127 cm^{-1} belongs to flake region and shows Nb–C vibrations. The in-plane symmetric vibrations in the region near 260 cm^{-1} are identified as A_{1g} out-of-plane vibrations of the metal atoms. The region from 200 cm^{-1} to 500 cm^{-1} is associated with the outer layer of metal and carbon atoms, as well as the mixed functional groups. The region of 550 cm^{-1} to 800 cm^{-1} results from multiple in and out-of-plane carbon vibrations, with vibrations between 600 cm^{-1} and 800 cm^{-1} being denoted as asymmetric, appearing only in MXenes with terminations on surface[66],[67].

4.6 Fourier Transform Infrared Spectroscopy (FTIR)

The FTIR spectra of pristine Nb_2CT_x MXene and $\text{Nb}_2\text{CT}_x/\text{Ag}$ NPs nanocomposite were recorded in the wavenumber range of 350 cm^{-1} to 4000 cm^{-1} , as shown in Fig 35.

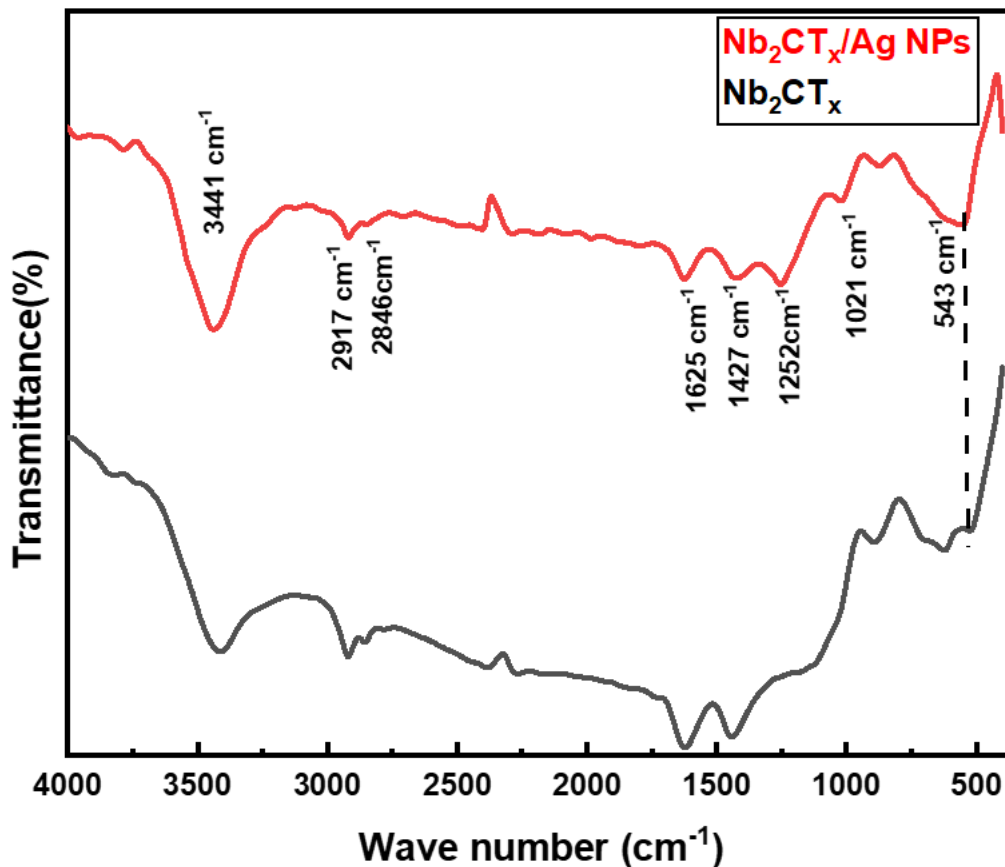


Figure 35: FTIR analysis of MXene and composite

The spectra can be divided into two regions: the functional group region (4000 cm^{-1} to 1000 cm^{-1}) and the fingerprint region (below 1000 cm^{-1}). The peak at 3441 cm^{-1} is attributed to O–H bond stretching vibrations, while the peaks at 2917 cm^{-1} , 2846 cm^{-1} correspond to C–H bonds stretching vibrations. The peaks observed at 1625 cm^{-1} , 1427 cm^{-1} , and 1021 cm^{-1} are associated with O–H bending vibrations, C–H bonds bending vibrations and C–O bonds stretching vibrations, respectively. The presence of a C–F band at 1252 cm^{-1} suggests asymmetric functionalization of the MXene sheets[68]. The $\text{Nb}_2\text{CT}_x/\text{Ag}$ NPs nanocomposite shows a higher density of surface

functional groups in comparison with pristine MXene, as confirmed by similar findings in the Raman data. The peak at 543 cm^{-1} in fingerprint region corresponds to the Nb–C mode of vibrations in MXene, and a similar but more intense peak in the composite material further indicates the successful synthesis of the nanocomposite[66],[69].

4.7 Photocatalytic Degradation and UV VIS Spectroscopic Analysis

Upon visible light irradiation, electron-hole pairs are generated, producing O_2 and OH radicals. These highly reactive radicals initiate the degradation of organic pollutants in the water solution, reducing them to harmless by-products, such as CO_2 and H_2O . In the general mechanism, photoexcited MXene and MXene based composite generate electron-hole pair charge carriers. The attached MXene sheets offer numerous trapping sites for electrons, which may increase the recombination rate of charge carriers as desired. Once the process begins, superoxide anion radicals ($\bullet\text{O}_2^-$) are produced, and concurrently $\bullet\text{OH}^-$ radicals are generated from the reaction of OH^- with holes. As the electrons interact with the photocatalyst, H_2O molecules are converted into OH radicals. These produced radicals, $\bullet\text{O}_2^-$, $\bullet\text{OH}^-$, being highly reactive towards organic pollutants degrade them into the harmless by-products CO_2 and H_2O .

4.7.1 Tauc Plot of MXene and Nanocomposites using UV/Vis Spectroscopy

We synthesized different composites of MXene and silver nanoparticles by using different ratios of silver nitrate salt by keeping the fixed amount of MXene. We synthesized composites by taking 25mg, 50mg and 75mg of silver nitrate salt with 100mg MXene for every composite. So, we named them as 1:0.25(C₁), 1:0.5(C₂) and 1:0.75(C₃). We then tested these photocatalyst by taking in different concentrations(3mg,15mg,30mg) against 10ppm antibiotic contaminated solution.

4.7.1.2 Band Gap Engineering

UV-VIS spectroscopy was employed to examine the optical properties of the synthesized materials. The optical band gap, measured using the Tauc plot, shows an increase in absorbance when Ag NPs are doped into MXene, effectively altering its band gap. The direct optical band gap of Nb_2CT_x MXene decreases from 1.80 eV to 1.52 eV, 1.46 eV, and 1.31 eV as the Ag NP doping

increases to 25%, 50%, and 75%, respectively. This reduction in band gap is likely due to the introduction of charge carriers by Ag NPs, which modify the band structure. A decrease in band gap suggests that photons with lower energy, corresponding to the visible region, can be absorbed more effectively[70]. The comparison of band gaps of MXene and composites are shown in fig 36(a), (b), (c) and (d).

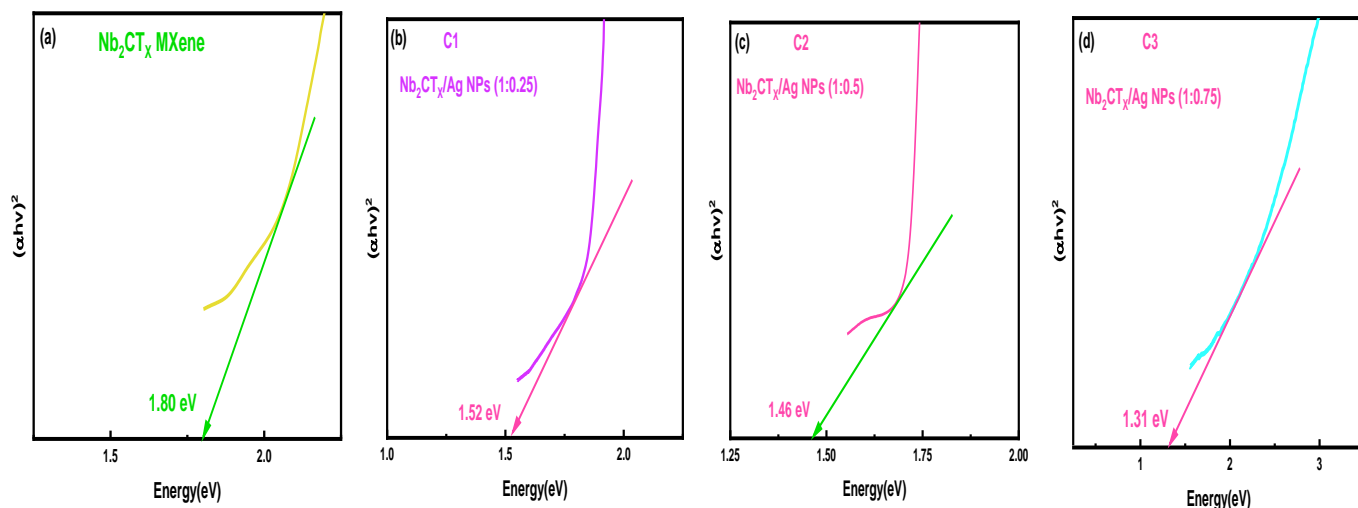


Figure 36: Band gap of (a) MXene (b) C1 (c) C2 (d) C3

4.7.2 Photocatalytic Activity of MXene and Nanocomposites

The photocatalytic performance of the MXene and nanocomposites made from MXene and silver nanoparticles was evaluated by measuring the degradation of antibiotic molecules in an aqueous solution. Norfloxacin and fleroxacin, both belonging to the fluoroquinolone group, were chosen for this study. The maximum wavelength (λ_{max}) of the antibiotic molecules was determined using a UV/Vis spectrophotometer. The degradation of the antibiotics was assessed by the photointensity of absorption of the nanocrystals of the synthesized composites, reflecting the remaining antibiotic molecules. A 400 W light bulb (Halogen Lamp), emitting radiation in the wavelength range of 315 nm to 400 nm (VIS region), was used as the light source to initiate the photocatalytic process. The bulb was positioned approximately 15 cm above the beaker containing the solution for analysis.

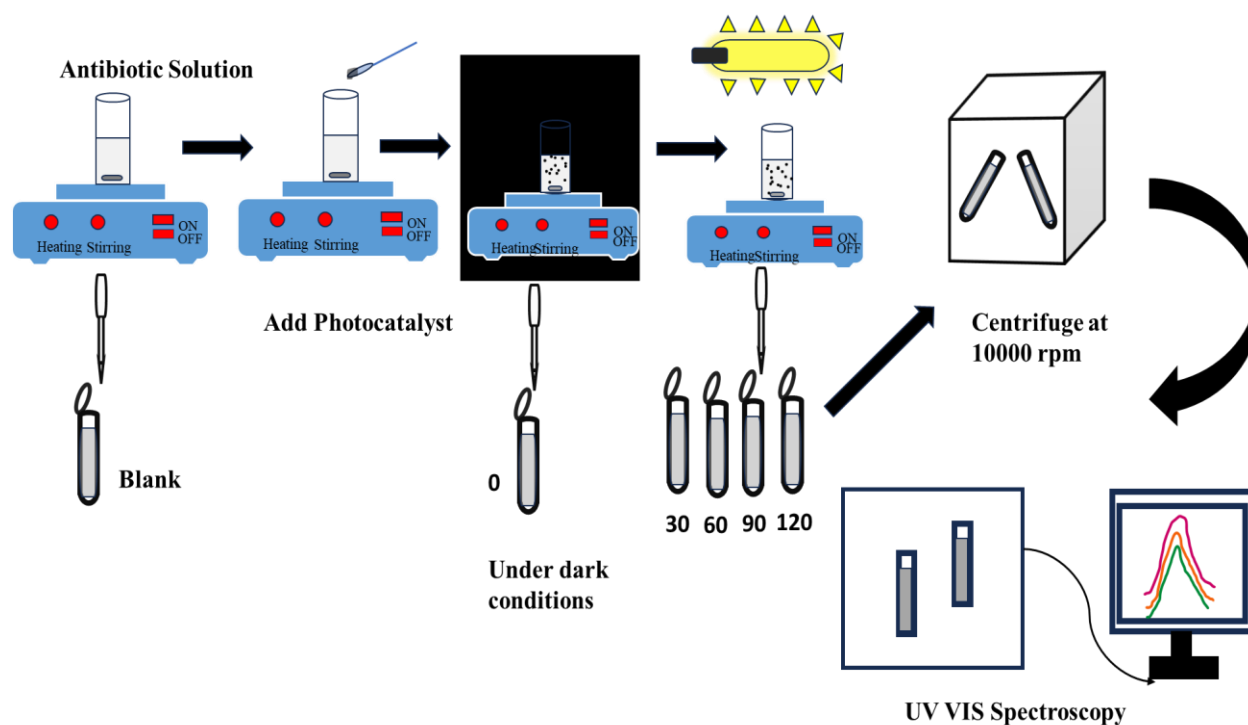


Figure 37: Photocatalytic Activity Testing.

According to the typical protocol of experiment, 100 mL of an antibiotic solution with a concentration of x ppm ($x=10$ ppm) was prepared. To this solution, y mg ($y=3,15,30$) of the photocatalyst was added, and the degradation of the antibiotic was monitored. The experiment began by adding y mg of the photocatalyst to the x ppm antibiotic solution. The solution was kept stirring under dark conditions for approximately 30 minutes to ensure adsorption-desorption equilibrium. After establishing equilibrium, the solution was placed under light source. Samples of 2 ml were taken at regular 30-minute intervals to measure antibiotic degradation. The samples were separated by centrifuge at 10000 rpm. Then the supernatant is analyzed by measuring the maximum absorbance using double beam UV VIS spectrophotometer.

The experiment was conducted by varying the concentrations of the photocatalyst in the antibiotic solution. The antibiotic solution was maintained at a concentration of 10 ppm, while the photocatalyst concentrations were adjusted to 3 mg, 15 mg, and 30 mg.

Norfloxacin and Fleroxacin Antibiotics

Norfloxacin and fleroxacin belong to quinolone/fluoroquinolone antibiotic family used for the treatment of bacterial infections. To prepare the 10ppm solution of antibiotic, we add 10mg of antibiotic in 1000ml(1L) of DI or 1mg in 100ml (0.1L) of DI and stir this solution for few minutes to make a homogenous antibiotic contaminated solution. We took 2ml solution in the vial to check the initial antibiotic concentration in the solution and nominated it as blank or -30.

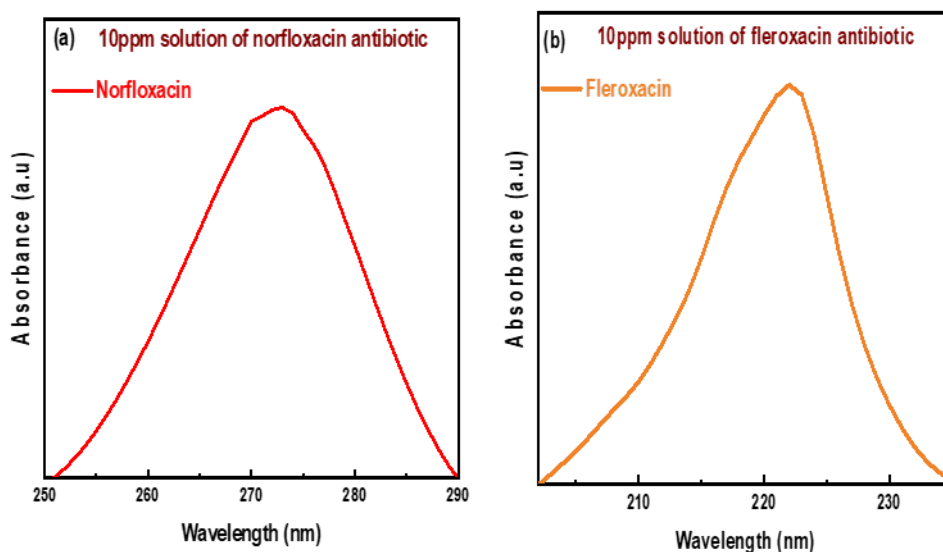


Figure 38: UV/Vis Spectra of 10ppm antibiotic solutions of (a) Norfloxacin (b) Fleroxacin.

4.7.2.1 Photocatalytic Degradation of Norfloxacin using MXene as Photocatalyst

We used MXene as a photocatalyst to check the degradation of antibiotic in solution. We divided it in 3 cases.

Case 1: In the 1st case, we put 3mg of MXene as photocatalyst in 30ml of 10ppm antibiotic solution to check the degradation of antibiotic. The solution was kept stirring for 30 minutes under dark conditions till the adsorption-desorption equilibrium had established.

Then the solution was illuminated by halogen lamp to start the photocatalysis process and took the 2ml solution in the vials to check the degradation of antibiotic in the solution after regular intervals of 30 minutes. Then all the samples were centrifuged at 10000 rpm and supernatant was analyzed.

It was observed that approximately **38%** degradation of antibiotic in the solution has taken place using UV-VIS Spectrophotometer.

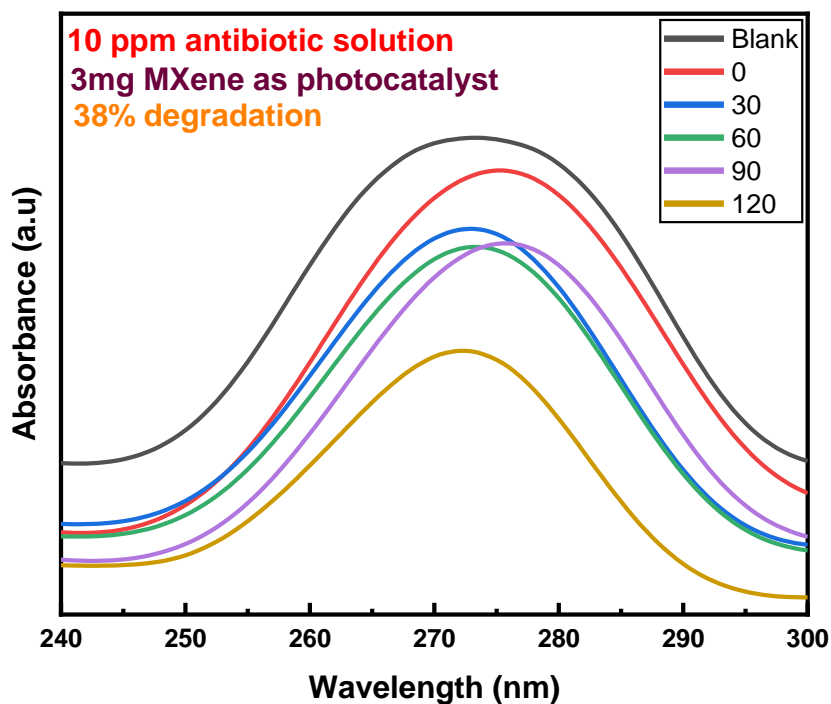


Figure 39: Photocatalytic degradation by Pristine MXene case 1.

The degradation was calculated using the following formula.

$$\%age\ Degradation = \{(C_0 - C_i) / C_0\} \times 100$$

Where, C_0 is the initial concentration of antibiotic in the solution and C_i is the concentration of antibiotic molecules at any instant in the solution. The graphical illustration of this case is shown in the Fig 39.

Case 2: In the 2nd case, we put 15mg MXene as photocatalyst in the 30ml of 10ppm antibiotic solution and kept stirring for half hour to attain the adsorption and desorption equilibrium under conditions. Then degradation of antibiotic molecules in solution was checked after regular intervals of 30 minutes by taking 2ml solution in vials. It was observed that **43%** antibiotic has been degraded. The graphical illustration of this case is shown in Fig 40.

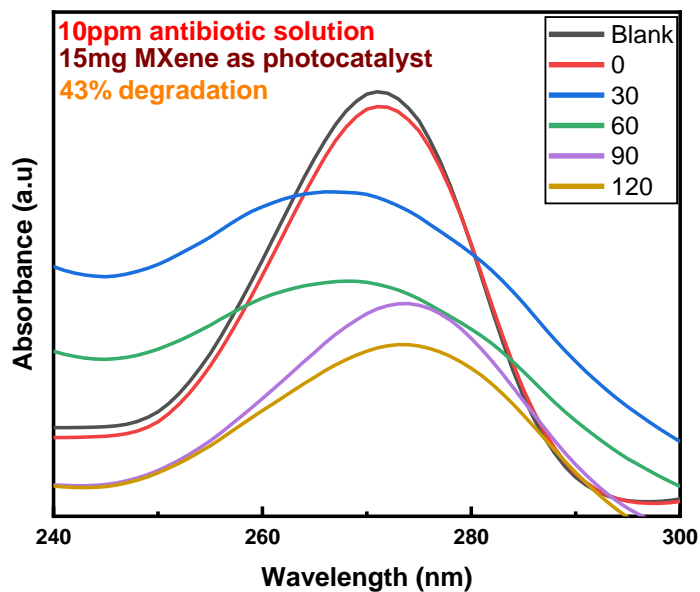


Figure 40: Photocatalytic degradation by pristine MXene case 2.

Case 3: In the 3rd case, we put 30 mg MXene in antibiotic solution and repeat the same process as in case 1 and 2. It was observed that 41% antibiotic has been degraded. The graphical illustration of this case is shown in Fig 41.

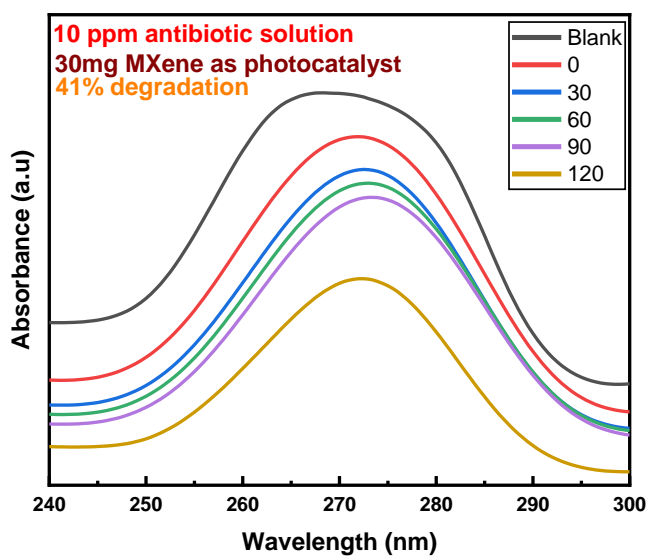


Figure 41: Photocatalytic degradation by pristine MXene case 3.

4.7.2.2 Photocatalytic Degradation of Norfloxacin using Nb₂C-Ag NPs as Photocatalyst

4.7.1.2.1 Degradation using C₁(1:0.25)

We synthesized nanocomposite using 100mg MXene and 25mg silver nitrate salt and tested this photocatalyst by using different concentrations i.e. 3mg, 15mg and 30mg.

Case 1: In the 1st case, we put 3mg of C₁ as photocatalyst in 30ml of 10ppm antibiotic solution to check the degradation of antibiotic. The solution was kept stirring for half hour under dark conditions till the adsorption and desorption equilibrium had been established. After that, solution was illuminated by halogen lamp to start the photocatalysis process and took the 2ml solution in the vials to check the degradation of antibiotic in the solution after regular intervals of 30 minutes.

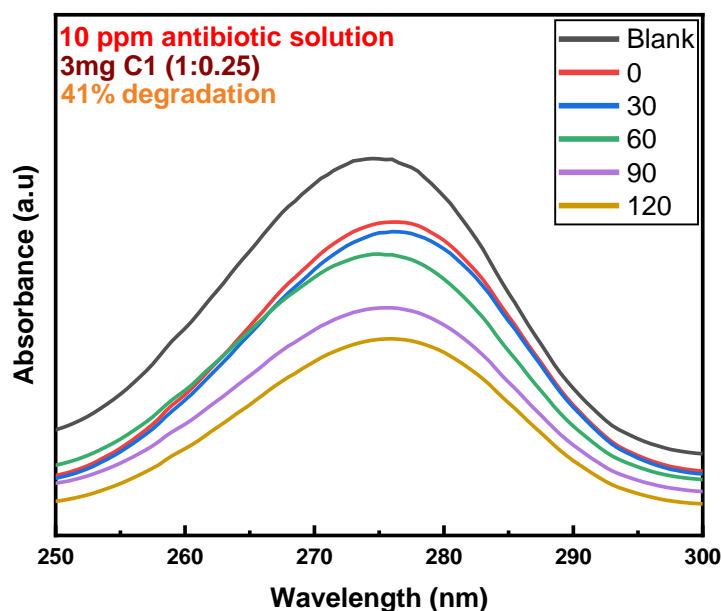


Figure 42: Photocatalytic degradation by C₁ case 1.

Then all the samples were centrifuged at 10000 rpm and supernatant was analyzed. It was observed that approximately 41% degradation of antibiotic in the solution has taken place using UV-VIS Spectrophotometer in fig 42.

Case 2: In the 2nd case, we put 15mg C₁ as photocatalyst in the 30ml of 10ppm antibiotic solution and kept on stirring for half hour to attain the adsorption and desorption equilibrium under dark conditions. Then degradation of antibiotic molecules in solution was checked after regular

intervals of 30 minutes by taking 2ml solution in vials. It was observed that **50%** antibiotic has been degraded. The graphical illustration of this case is shown in Fig 43.

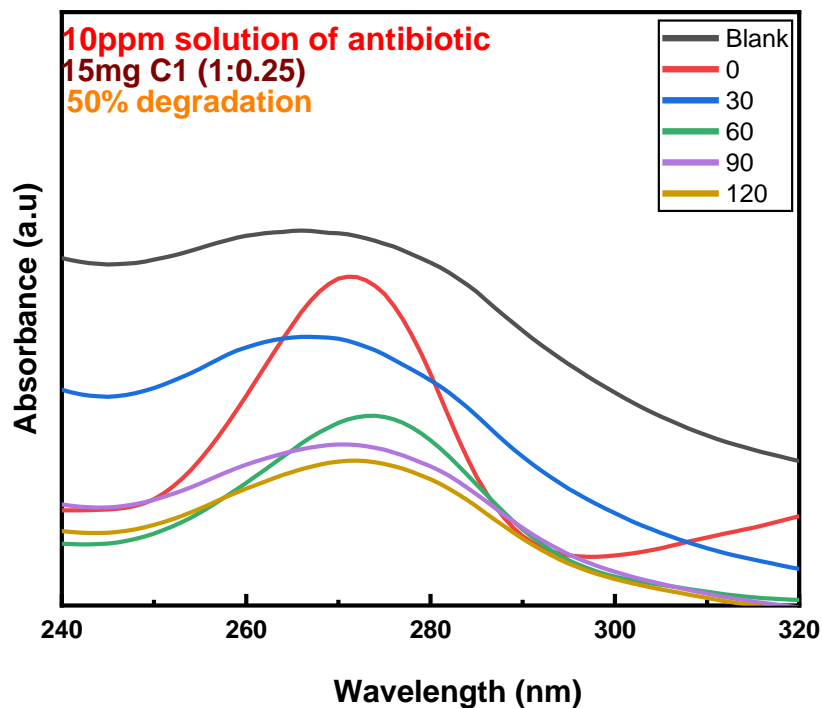


Figure 43: Photocatalytic degradation by C1 case 2.

Case 3: In the 3rd case, we put 30mg C₁ in antibiotic solution and repeat the same process as in case 1 and 2. It was observed that **47%** antibiotic has been degraded. The graphical illustration of this case is shown in Fig 44.

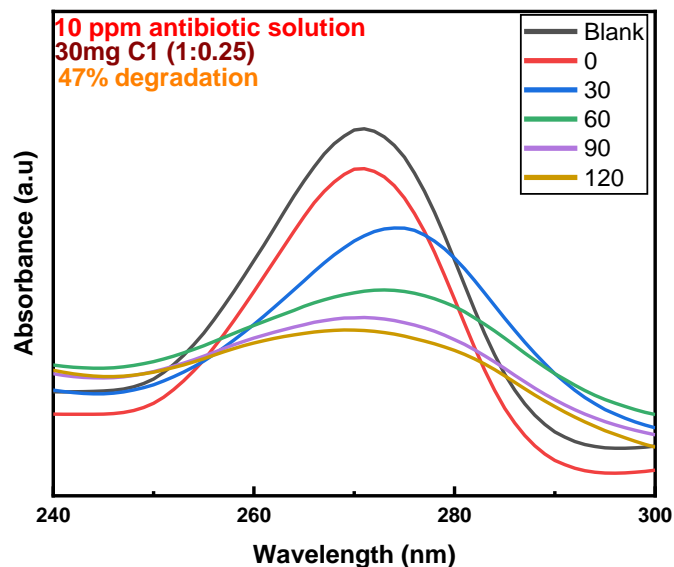


Figure 44: Photocatalytic degradation by C1 case 3.

4.7.2.2.2 Degradation using C₂(1:0.5)

We synthesized nanocomposite using 100mg MXene and 50mg silver nitrate salt and tested this photocatalyst by using different concentrations i.e. 3mg, 15mg and 30mg.

Case 1: In the 1st case, we put 3mg of C₂ as photocatalyst in 30ml of 10ppm antibiotic solution to check the degradation of antibiotic. The solution was kept on stirring for half hour under dark conditions for the adsorption-desorption equilibrium established.

Then the solution was illuminated by halogen lamp to start the photocatalysis process and took the 2ml solution in the vials to check the degradation of antibiotic in the solution after regular intervals of 30 minutes. Then all the samples were centrifuged at 10000 rpm and supernatant was analyzed. It was observed that approximately **52.16%** degradation of antibiotic in the solution has taken place using UV-VIS Spectrophotometer. The graphical illustration of this case is shown in Fig 45.

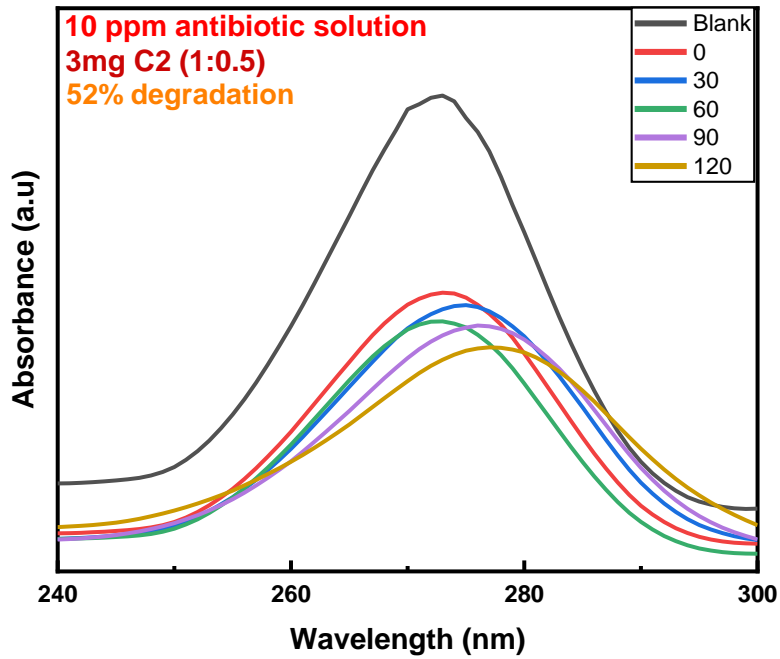


Figure 45: Photocatalytic degradation by C2 case 1.

Case 2: In the 2nd case, we put 15mg C2 as photocatalyst in the 30ml of 10ppm antibiotic solution and stirred for 30 minutes to attain the adsorption-desorption equilibrium under conditions.

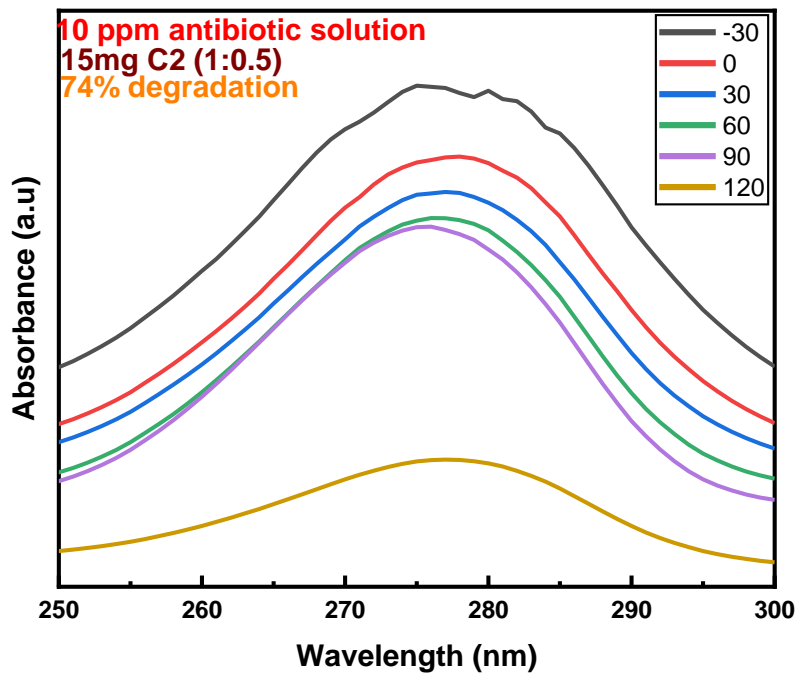


Figure 46: Photocatalytic degradation by C2 case 2.

Then the degradation of antibiotic molecules in solution was checked after regular intervals of 30 minutes by taking 2ml solution in vials. It was observed that **74.49%** antibiotic has been degraded. The graphical illustration of this case is shown in Fig 46.

Case 3: In the 3rd case, we put 30mg C₂ in antibiotic solution and repeat the same process as in case 1 and 2.

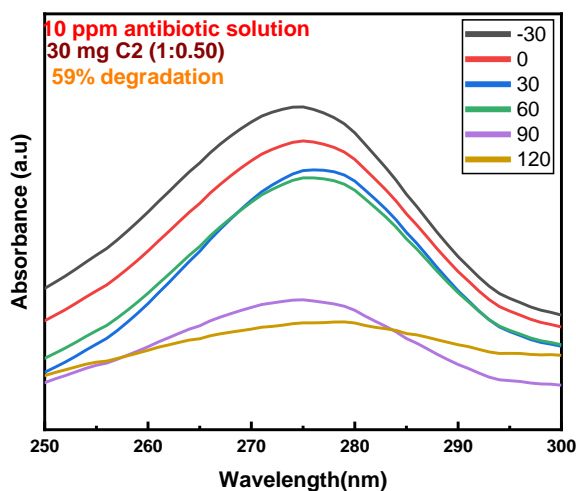


Figure 47: Photocatalytic degradation by C₂ case 3.

It was observed that **59%** antibiotic has been degraded. The graphical illustration of this case is shown in Fig 47.

4.7.2.2.3 Degradation using C₃(1:0.75)

We synthesized nanocomposite using 100mg MXene and 75mg silver nitrate salt and tested this photocatalyst by using different concentrations i.e. 3mg, 15mg and 30mg.

Case 1: In the 1st case, we put 3mg of C₃ as photocatalyst in 30ml of 10ppm antibiotic solution to check the degradation of antibiotic. The solution was kept stirring for half hour under dark conditions till the adsorption and desorption equilibrium was established.

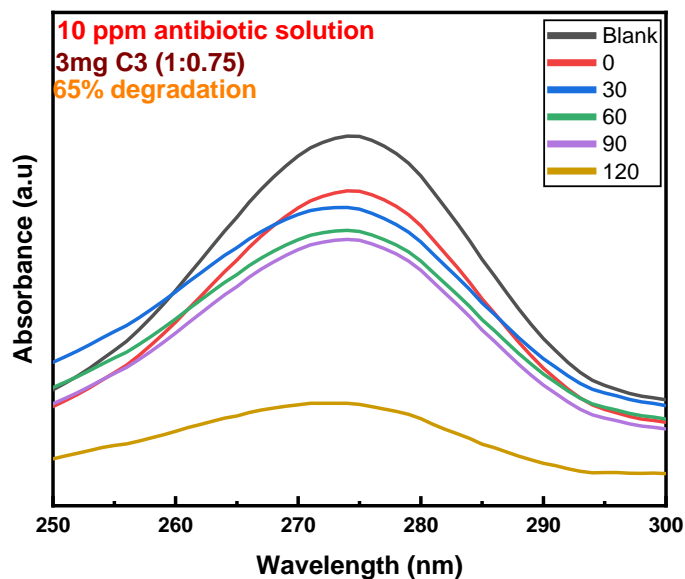


Figure 48: Photocatalytic degradation by C3 case 1.

Then the solution was illuminated by halogen lamp to start the photocatalysis process and took the 2ml solution in the vials to check the degradation of antibiotic in the solution after regular intervals of 30 minutes. Then all the samples were centrifuged at 10000 rpm and supernatant was analyzed. It was observed that approximately **65%** degradation of antibiotic in the solution has taken place using UV-VIS Spectrophotometer.

Case 2: In the 2nd case, we put 15mg C₃ as photocatalyst in the 30ml of 10ppm antibiotic solution and stirred for 30 minutes to attain the adsorption-desorption equilibrium under conditions.

Then the degradation of antibiotic molecules in solution was checked after regular intervals of 30 minutes by taking 2ml solution in vials. It was observed that **70%** antibiotic has been degraded. The graphical illustration of this case is shown in Fig 49.

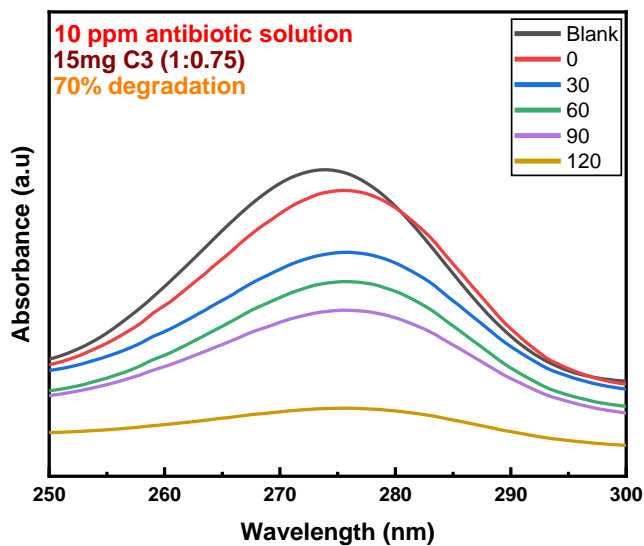


Figure 49: Photocatalytic degradation by C3 case 2.

Case 3: In the 3rd case, we put 30mg C₃ in antibiotic solution and repeat the same process as in case 1 and 2.

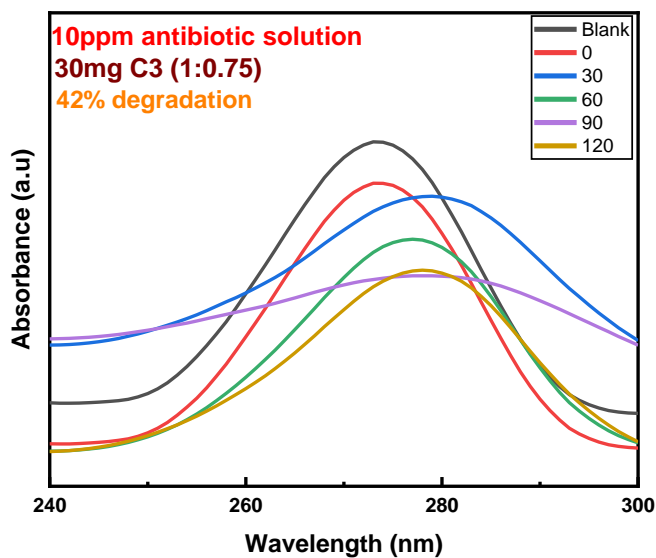


Figure 50: Photocatalytic degradation by C3 case 3.

It was observed that **42%** antibiotic has been degraded. The graphical illustration of this case is shown in Fig 50.

4.7.2.3 Kinetic Study of Photocatalytic degradation of Norfloxacin Antibiotic

The rate constant for the degradation data was determined, and the reaction was found to adhere to the equation for a pseudo-first-order reaction, expressed as:

$$\ln(C_0/C_i) = kT$$

Here, C_0 represents the initial concentration of the dye, C_i is the concentration of the dye at any given time, T is the illumination time, and k is the rate constant of the reaction. The kinetic constants for MXene and all the nanocomposites are shown in Fig 51.

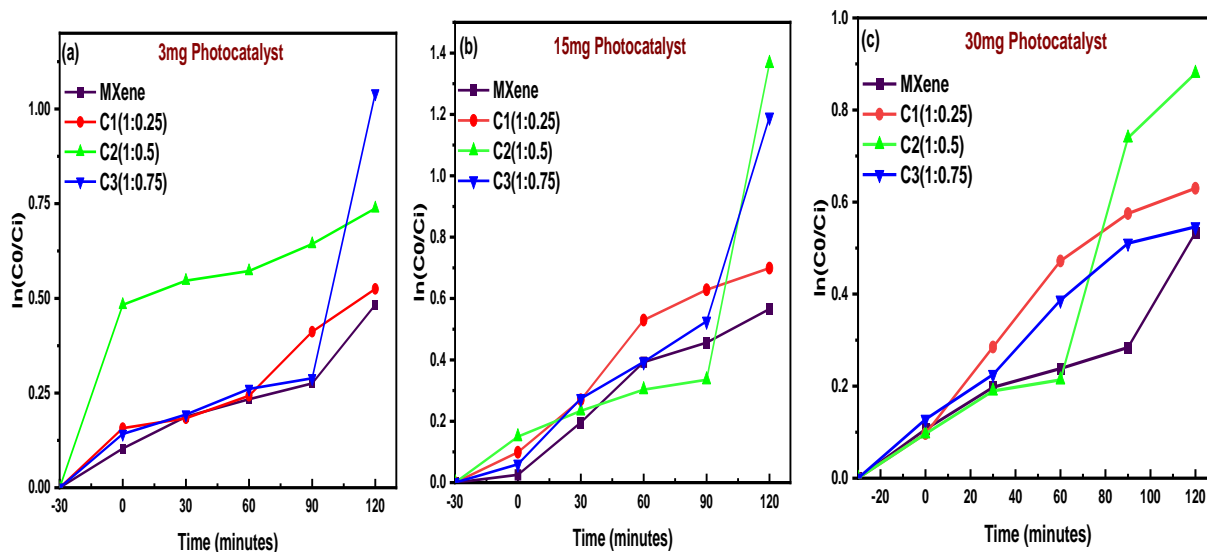


Figure 51: Kinetic studies of MXene and nanocomposites (a) with 3mg (b) with 15mg (c) with 30mg.

The rate constant values for 3 mg of photocatalysts Nb₂CTx MXene, C₁ (1:0.25), C₂ (1:0.5) and C₃ (1:0.75) were calculated to be 0.008552 m⁻¹, 0.010134 m⁻¹, 0.019884 m⁻¹, 0.012838 m⁻¹ respectively when the concentration of norfloxacin antibiotic solution was 10 ppm shown in Fig

The rate constant values for 15 mg of photocatalysts Nb₂CTx MXene, C₁ (1:0.25), C₂ (1:0.5) and C₃ (1:0.75) were calculated to be 0.013427 m⁻¹, 0.014842 m⁻¹, 0.036028 m⁻¹, 0.01629 m⁻¹ respectively when the concentration of norfloxacin antibiotic solution was 10 ppm shown in Fig.

The rate constant values for 30 mg of photocatalysts Nb₂CTx MXene, C₁ (1:0.25), C₂ (1:0.5) and C₃ (1:0.75) were calculated to be 0.009064 m⁻¹, 0.013718 m⁻¹, 0.014126 m⁻¹, 0.011978 m⁻¹

respectively when the concentration of norfloxacin antibiotic solution was 10 ppm shown in Fig 51.

The highest value of the rate constant was approximately $0.036028 \text{ min}^{-1}$ for 15mg Nb₂CT_x/Ag NPs (C₂(1:0.5)) photocatalyst added in the 10ppm solution of norfloxacin antibiotic. This value of rate constant is in correspondence to the maximum photodegradation activity of **74%** when 15mg Nb₂CT_x/Ag NPs was added in 10ppm antibiotic solution. The overall photocatalytic results showed that MXene and nanocomposites C₁ and C₃ exhibited appreciable photocatalytic ability to degrade norfloxacin antibiotic solution.

4.7.2.4 Photocatalytic Degradation of Fleroxacin using MXene as Photocatalyst

We used MXene as a photocatalyst to check the degradation of antibiotic in solution. We divided it in 3 cases.

Case 1: In the 1st case, we put 3mg of MXene as photocatalyst in 30ml of 10ppm antibiotic solution to check the degradation of antibiotic. The solution was kept on stirring for half hour under dark conditions until the adsorption and desorption equilibrium was established. Then solution was illuminated by halogen lamp to start the photocatalysis process and took the 2ml solution in the vials to check the degradation of antibiotic in the solution after regular intervals of 30 minutes.

Then all the samples were centrifuged at 10000 rpm and supernatant was analyzed. It was observed that approximately **31.35%** degradation of antibiotic in the solution has taken place using UV-VIS Spectroscopy. The degradation was calculated using the following formula.

$$\text{\%age Degradation} = \{(C_0 - C_i) / C_0\} \times 100$$

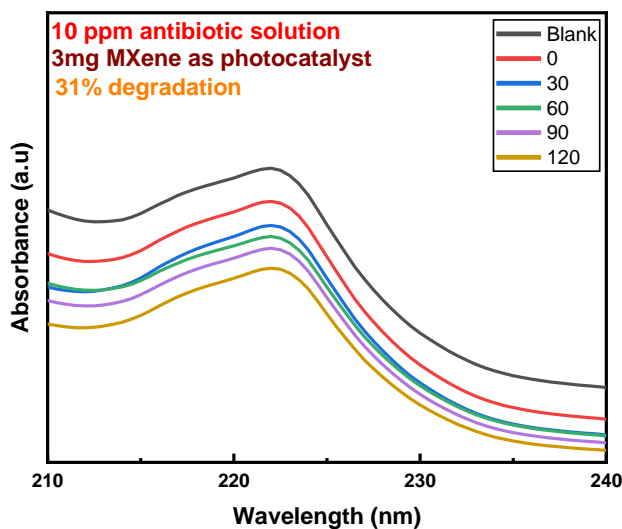


Figure 52: Photocatalytic degradation by pristine MXene case 1.

Where, C_0 is the initial concentration of antibiotic in the solution and C_i is the concentration of antibiotic molecules at any instant in the solution. The graphical illustration of this case is shown in the Fig 52.

Case 2: In the 2nd case, we put 15mg MXene as photocatalyst in the 30ml of 10ppm antibiotic solution and kept on stirring for half hour to attain the adsorption and desorption equilibrium under dark conditions.

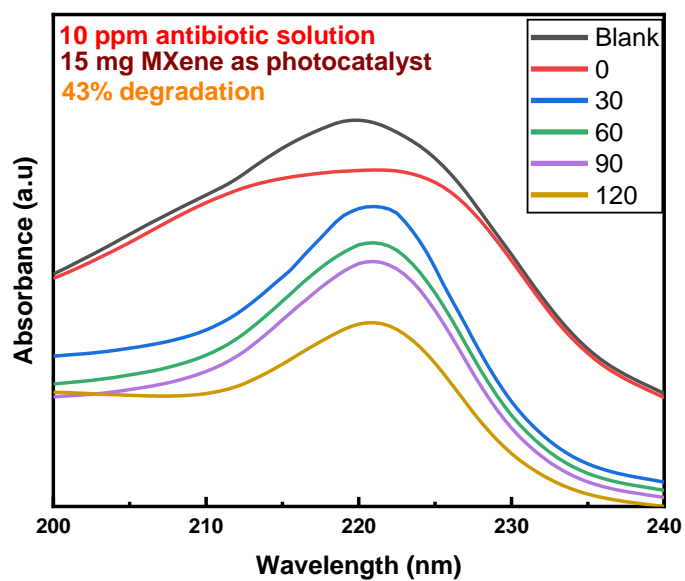


Figure 53: Photocatalytic degradation by pristine MXene case 2.

Then degradation of antibiotic molecules in solution was checked after regular intervals of 30 minutes by taking 2ml solution in vials. It was observed that **43.11%** antibiotic has been degraded. The graphical illustration of this case is shown in Fig 53.

Case 3: In the 3rd case, we put 30mg MXene in antibiotic solution and repeat the same process as in case 1 and 2. It was observed that **31%** antibiotic has been degraded. The graphical illustration of this case is shown in Fig 54.

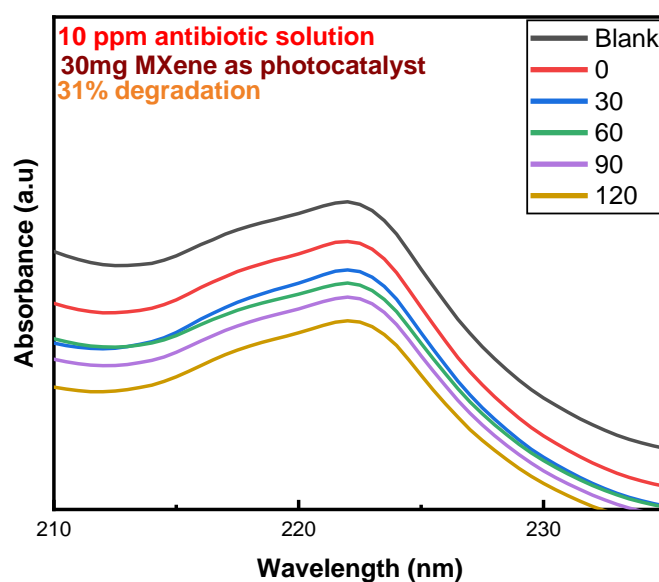


Figure 54: Photocatalytic degradation by pristine MXene case 3.

4.7.2.5 Photocatalytic Degradation of Fleroxacin using Nb₂C-Ag NPs as Photocatalyst

We synthesized different composites of MXene and silver nanoparticles by using different ratios of silver nitrate salt by keeping the fixed amount of MXene. We synthesized composites by taking 25mg, 50mg and 75mg of silver nitrate salt with 100mg MXene for every composite. So, we named them as 1:0.25(C₁), 1:0.5(C₂) and 1:0.75(C₃). We then tested these photocatalyst by taking in different concentrations(3mg,15mg,30mg) against 10ppm antibiotic contaminated solution.

4.7.2.5.1 Degradation using C₁(1:0.25)

We synthesized nanocomposite using 100mg MXene and 25mg silver nitrate salt and tested this photocatalyst by using different concentrations i.e. 3mg, 15mg and 30mg.

Case 1: In the 1st case, we put 3mg of C₁ as photocatalyst in 30ml of 10ppm antibiotic solution to check the degradation of antibiotic. The solution was kept on stirring for half hour under dark conditions for the adsorption-desorption equilibrium established.

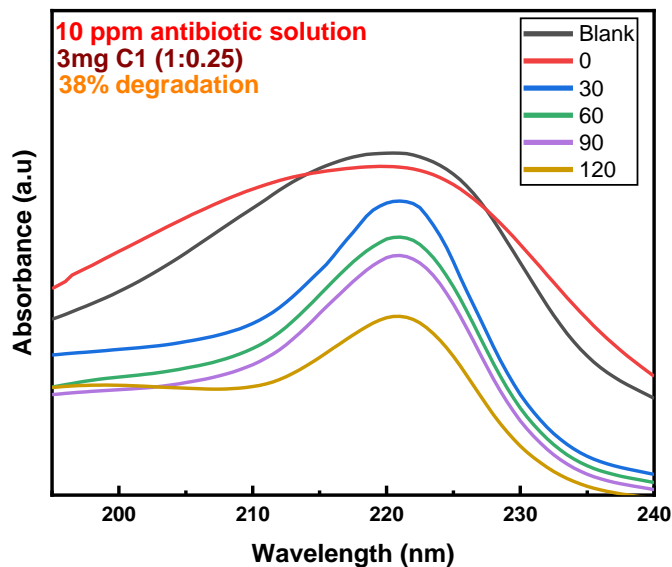


Figure 55: Photocatalytic degradation by C₁ case 1.

Then the solution was illuminated by halogen lamp to start the photocatalysis process and took the 2ml solution in the vials to check the degradation of antibiotic in the solution after regular intervals of 30 minutes. Then all the samples were centrifuged at 10000 rpm and supernatant was analyzed. It was observed that approximately **38%** degradation of antibiotic in the solution has taken place using UV-VIS Spectrophotometer.

Case 2: In the 2nd case, we put 15mg C₁ as photocatalyst in the 30ml of 10ppm antibiotic solution and kept on stirring for half hour to attain the adsorption and desorption equilibrium under dark conditions. Then the degradation of antibiotic molecules in solution was checked after regular intervals of 30 minutes by taking 2ml solution in vials. It was observed that **55%** antibiotic has been degraded. The graphical illustration of this case is shown in Fig 56.

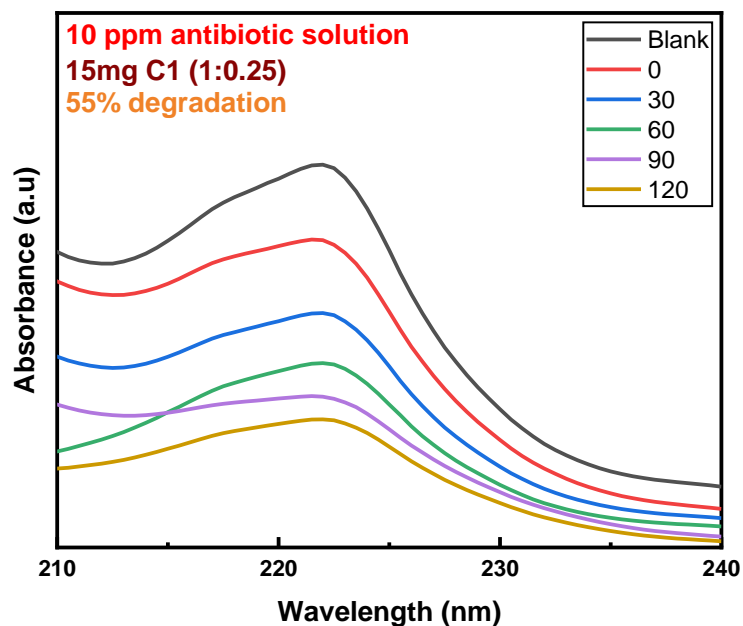


Figure 56: Photocatalytic degradation by C1 case 2.

Case 3: In the 3rd case, we put 30mg C1 in antibiotic solution and repeat the same process as in case 1 and 2. It was observed that 44% antibiotic has been degraded. The graphical illustration of this case is shown in Fig 57.

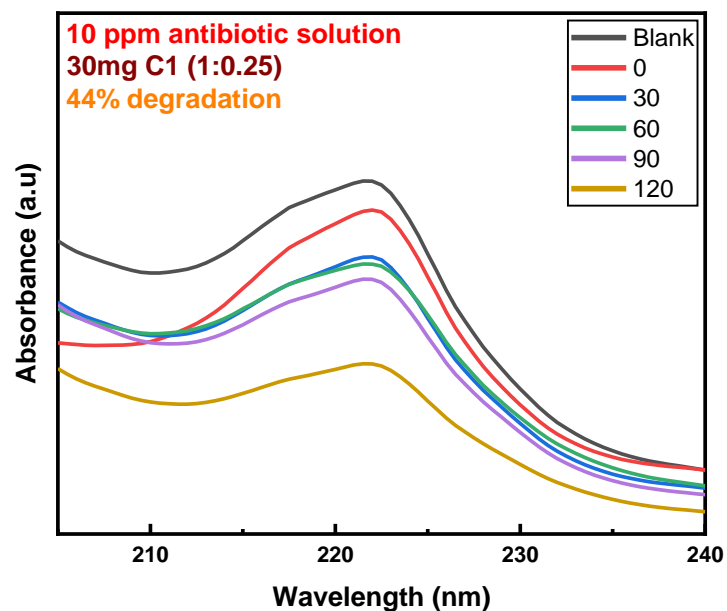


Figure 57: Photocatalytic degradation by C1 case 3.

4.7.2.5.2 Degradation using C₂(1:0.5)

We synthesized nanocomposite using 100mg MXene and 50mg silver nitrate salt and tested this photocatalyst by using different concentrations i.e. 3mg, 15mg and 30mg.

Case 1: In the 1st case, we put 3mg of C₂ as photocatalyst in 30ml of 10ppm antibiotic solution to check the degradation of antibiotic. The solution was kept on stirring for half hour under dark conditions until the adsorption and desorption equilibrium was established. The solution was then illuminated by halogen lamp to start the photocatalysis process and took the 2ml solution in the vials to check the degradation of antibiotic in the solution after regular intervals of 30 minutes.

Then all the samples were centrifuged at 10000 rpm and supernatant was analyzed. It was observed that approximately 57% degradation of antibiotic in the solution has taken place using UV-VIS Spectrophotometer.

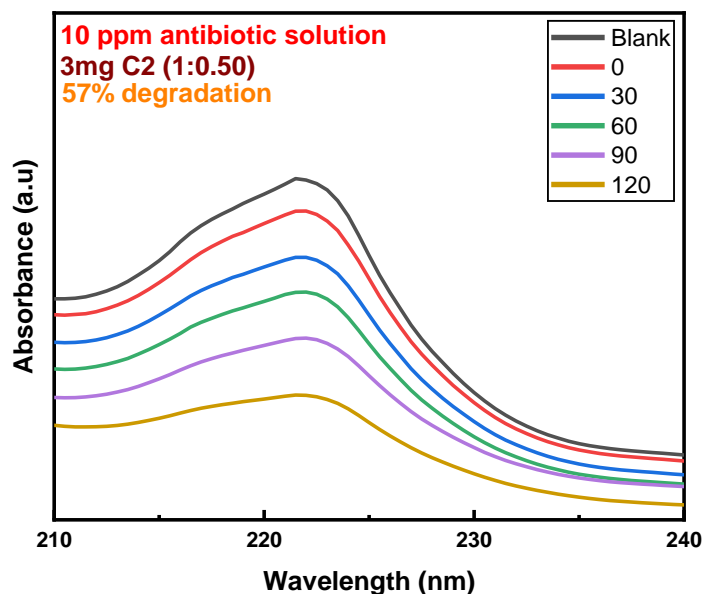


Figure 58: Photocatalytic degradation by C₂ case 1.

Case 2: In the 2nd case, we put 15mg C₂ as photocatalyst in the 30ml of 10ppm antibiotic solution was stirred for half hour to attain the adsorption and desorption equilibrium under conditions.

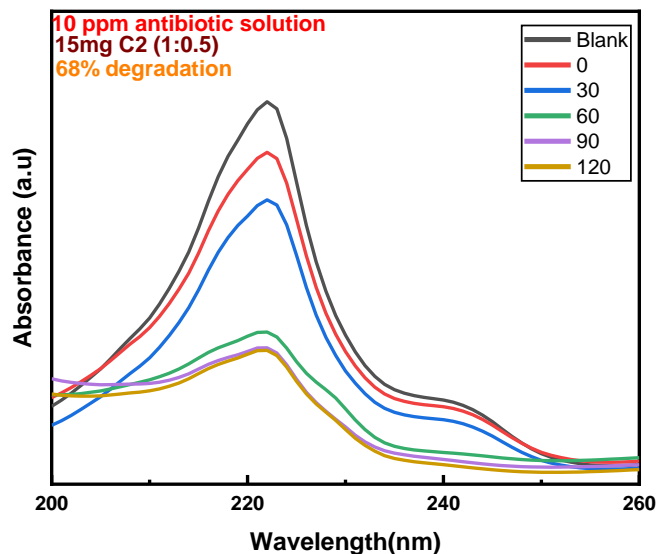


Figure 59: Photocatalytic degradation by C2 case 2.

Then degradation of antibiotic molecules in solution was checked after regular intervals of 30 minutes by taking 2ml solution in vials. It was observed that **68%** antibiotic has been degraded. The graphical illustration of this case is shown in Fig 59.

Case 3: In the 3rd case, we put 30mg C2 in antibiotic solution and repeat the same process as in case 1 and 2. It was observed that **63%** antibiotic has been degraded. The graphical illustration of this case is shown in Fig 60.

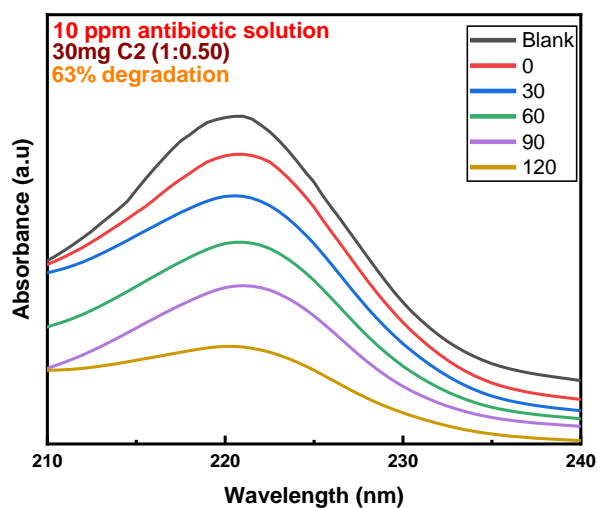


Figure 60: Photocatalytic degradation by C2 case 3.

4.7.2.5.3 Degradation using C₃(1:0.75)

We synthesized nanocomposite using 100mg MXene and 75mg silver nitrate salt and tested this photocatalyst by using different concentrations i.e. 3mg, 15mg and 30mg.

Case 1: In the 1st case, we put 3mg of C₃ as photocatalyst in 30ml of 10ppm antibiotic solution to check the degradation of antibiotic. The solution was kept on stirring for half hour under dark conditions till the adsorption and desorption equilibrium had been established.

Then the solution was illuminated by halogen lamp to start the photocatalysis process and took the 2ml solution in the vials to check the degradation of antibiotic in the solution after regular intervals of 30 minutes. Then all the samples were centrifuged at 10000 rpm and supernatant was analyzed. It was observed that approximately **57%** degradation of antibiotic in the solution has taken place using UV-VIS Spectrophotometer in fig 61.

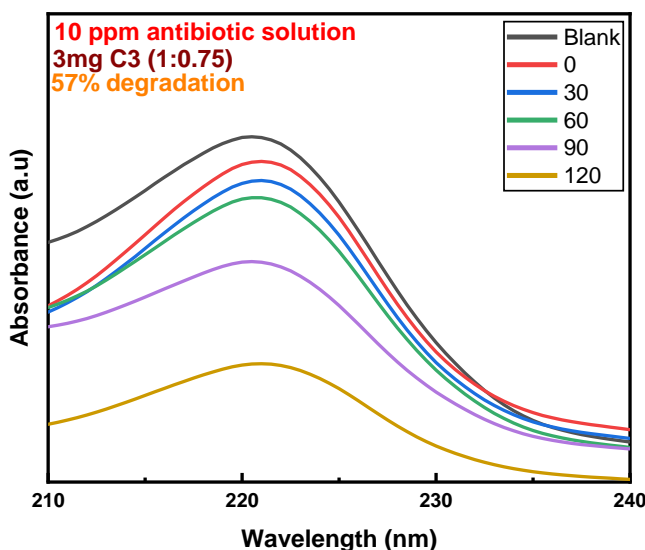


Figure 61: Photocatalytic degradation by C₃ case 1.

Case 2: In the 2nd case, we put 15mg C₃ as photocatalyst in the 30ml of 10ppm antibiotic solution and kept on stirring for half hour to maintain the adsorption-desorption equilibrium under conditions. Then the degradation of antibiotic molecules in solution was checked after regular intervals of 30 minutes by taking 2ml solution in vials. It was observed that **62.85%** antibiotic has been degraded. The graphical illustration of this case is shown in Fig 62.

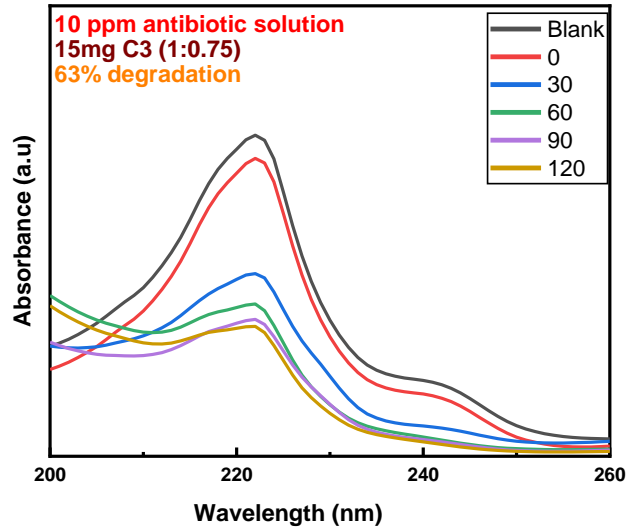


Figure 62: Photocatalytic degradation by C3 case 2.

Case 3: In the 3rd case, we put 30mg C₃ in antibiotic solution and repeat the same process as in case 1 and 2. It was observed that **60%** antibiotic has been degraded. The graphical illustration of this case is shown in Fig 63.

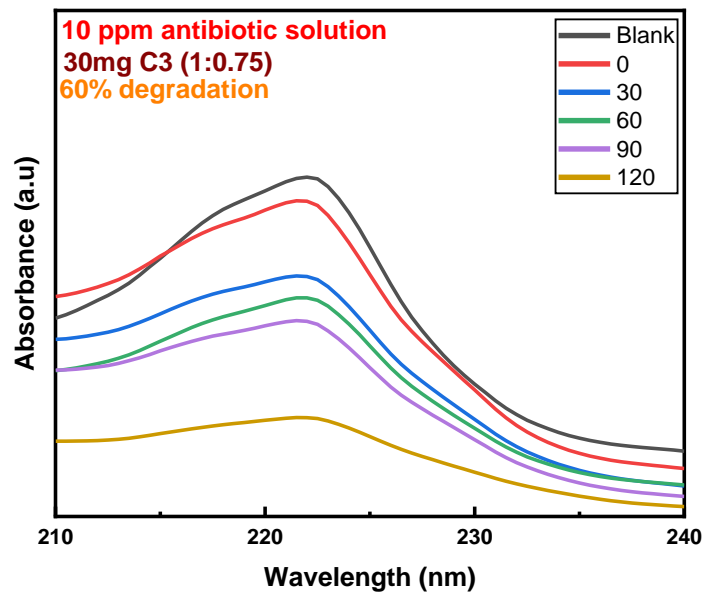


Figure 63: Photocatalytic degradation by C3 case 3.

4.7.2.6 Kinetic Study of Photocatalytic degradation of Fleroxacin Antibiotic

The rate constant for the degradation data was determined, and the reaction was found to adhere to the equation for a pseudo-first-order reaction, expressed as:

$$\ln(C_0/C_i) = kT$$

Here, C_0 represents the initial concentration of the dye, C_i is the concentration of the dye at any given time, T is the illumination time, and k is the rate constant of the reaction. The kinetic constants for MXene and all the nanocomposites are shown in Fig 64.

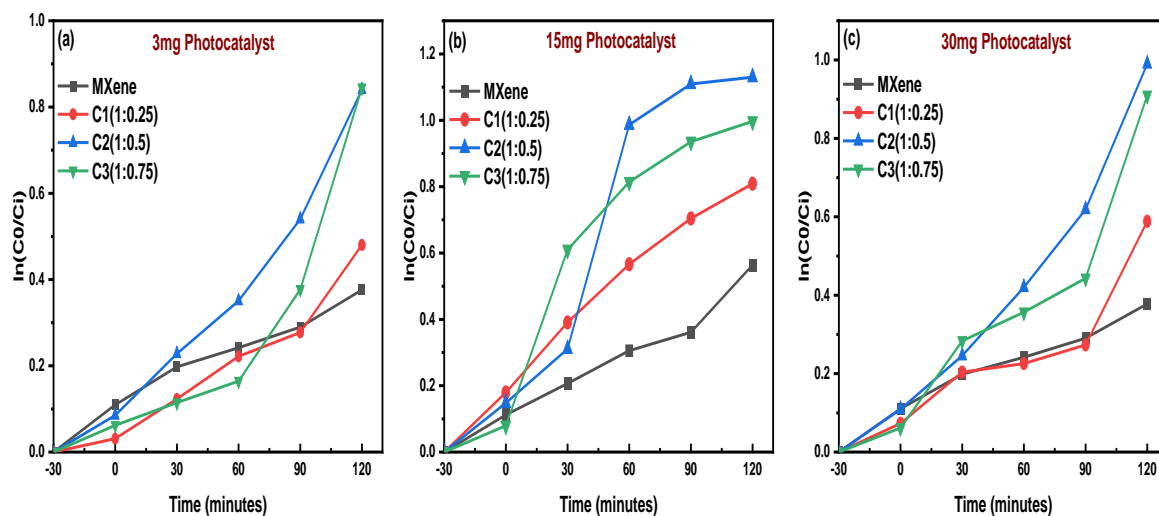


Figure 64: Kinetic studies of MXene and nanocomposites (a) with 3mg (b) with 15mg (c) with 30mg.

The rate constant values for 3 mg of photocatalysts Nb₂CTx MXene, C1 (1:0.25), C2 (1:0.5) and C3 (1:0.75) were calculated to be 0.008098 m⁻¹, 0.007554 m⁻¹, 0.013628 m⁻¹, 0.010418 m⁻¹ respectively when the concentration of fleroxacin antibiotic solution was 10 ppm shown in Fig

The rate constant values for 15 mg of photocatalysts Nb₂CTx MXene, C1 (1:0.25), C2 (1:0.5) and C3 (1:0.75) were calculated to be 0.008956 m⁻¹, 0.017664 m⁻¹, 0.024566 m⁻¹, 0.022908 m⁻¹ respectively when the concentration of fleroxacin antibiotic solution was 10 ppm shown in Fig 64.

The rate constant values for 30 mg of photocatalysts Nb₂CT_x MXene, C₁ (1:0.25), C₂ (1:0.5) and C₃ (1:0.75) were calculated to be 0.008128 m⁻¹, 0.009094 m⁻¹, 0.015894 m⁻¹, 0.013698 m⁻¹ respectively when the concentration of fleroxacin antibiotic solution was 10 ppm shown in Fig.

The highest value of the rate constant was approximately 0.024566 min⁻¹ for 15mg Nb₂CT_x/Ag NPs (C₂(1:0.5)) photocatalyst added in the 10ppm solution of fleroxacin antibiotic. This value of rate constant is in correspondence to the maximum photodegradation activity of **70%** when 15mg Nb₂CT_x/Ag NPs was added in 10ppm antibiotic solution. The overall photocatalytic results showed that MXene and nanocomposites C₁ and C₃ exhibited appreciable photocatalytic ability to degrade fleroxacin antibiotic solution.

4.8 Photoluminescence Spectra Analysis

Fig65 presents the PL spectra of pristine Nb₂CT_x MXene and Nb₂CT_x/Ag nanoparticles (Ag NPs) composites at various ratios. The pure Nb₂CT_x sample exhibits a primary emission peak around 451 nm. When compared to pristine Nb₂CT_x, the PL intensity of the Nb₂CT_x/Ag NPs composites decreases significantly at the same wavelength, indicating a lower charge recombination rate in the Nb₂CT_x/Ag NPs nanocomposites. Generally, a lower charge recombination rate corresponds to a reduced PL intensity, leading to enhanced photocatalytic activity.

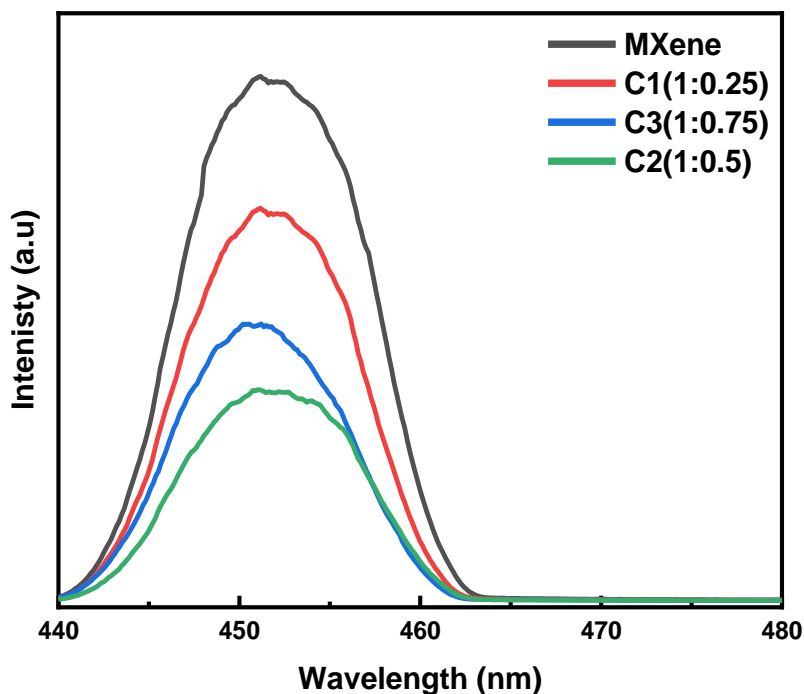


Figure 65: PL Spectra of Pristine MXene and nanocomposites.

In Fig 65, the black line represents the PL spectrum of the pristine Nb₂CT_x MXene. The higher PL intensity for this sample suggests a high charge recombination rate, which correlates with lower photocatalytic activity. Conversely, the green curve shows the lowest intensity values, corresponding to the lowest charge recombination rate. This reduced recombination rate enhances the photocatalytic activity, with the green curve representing the Nb₂CT_x/Ag NPs (1:0.5) composite. This sample demonstrates the highest photocatalytic activity, achieving 74% and 70% degradation for norfloxacin and fleroxacin antibiotics, respectively.

The red and blue curves in the figure represent the PL spectra for 25% and 75% Ag NPs doping in Nb₂CT_x MXene, respectively. Although these nanocomposites have a higher recombination rate and lower photocatalytic activity compared to the Nb₂CT_x/Ag NPs (1:0.5) composite, they still exhibit appreciable degradation results.

Conclusion

The two-dimensional (2D) MXene sheets were synthesized from their pure MAX phase (Nb_2AlC) by wet chemical etching method. Ag nanoparticles were synthesized using electrostatic self-assembly method. The synthesized MXene had narrow band gap of 1.80eV but to make it more effective for visible light we doped pristine mxene with 25%, 50% and 75% Ag NPs. The nanocomposites C1(1:0.25), C2(1:0.5) and C3(1:0.75) had narrower band gaps of 1.52eV, 1.46 eV and 1.31eV as compared to pristine MXene. The synthesized MXene and composites were further tested for photocatalytic degradation of norfloxacin and fleroxacin antibiotics and were proved to be the best photocatalysts under visible light irradiation which degraded the antibiotics up to 74% and 70% in only 120 minutes as compared to pristine MXene which showed degradation up to 38% and 31% respectively. With the increase in Ag NPs concentration the degrading efficiency has decreased. Efficient degradation to the best of our knowledge is due to lower charge recombination rate in composites. Also, the highest photocatalytic activity for antibiotics attained here without any co-catalyst is unique in itself, because it's very difficult to degrade antibiotics because of their strong chemical stability, which makes these nanocomposites a potential candidate for commercial applications owing to its low-cost synthesis route.

Future Perspective

My study on MXene, particularly in the field of photocatalyst, described in this dissertation will serve as a roadmap for scholars to go further into the growing field of 2D materials.

Development of safe and efficient green etching techniques for A layer removal at room temperature.

- Optimizing the amount of photocatalysts for enhanced degradation efficiency.
- Intercalating various nanoparticles into MXene for degradation of antibiotics and other harmful organic pollutants.
- Enhancing MXene-based photocatalysts for self-cleaning glass that are highly active under visible light, ensuring efficient degradation of organic pollutants and dirt.

References

- [1] S. Mobasser and A. A. Firoozi, “Review of Nanotechnology Applications in Science and Engineering,” 2016. [Online]. Available: www.ojceu.ir
- [2] A. Alagarasi, “Chapter-INTRODUCTION TO NANOMATERIALS.”
- [3] B. Mekuye and B. Abera, “Nanomaterials: An overview of synthesis, classification, characterization, and applications,” *Nano Select*, vol. 4, no. 8, pp. 486–501, Aug. 2023, doi: 10.1002/nano.202300038.
- [4] Paras *et al.*, “A Review on Low-Dimensional Nanomaterials: Nanofabrication, Characterization and Applications,” Jan. 01, 2023, *MDPI*. doi: 10.3390/nano13010160.
- [5] J. Theron, J. A. Walker, and T. E. Cloete, “Nanotechnology and water treatment: Applications and emerging opportunities,” Feb. 2008. doi: 10.1080/10408410701710442.
- [6] P. Punia *et al.*, “Recent advances in synthesis, characterization, and applications of nanoparticles for contaminated water treatment- A review,” Jan. 15, 2021, *Elsevier Ltd*. doi: 10.1016/j.ceramint.2020.09.050.
- [7] Zamathula Queen Sikhakhane Nwokediegwu, Onyeka Henry Daraojimba, Johnson Sunday Oliha, Alexander Obaigbena, Michael Ayorinde Dada, and Michael Tega Majemite, “Review of emerging contaminants in water: USA and African perspectives,” *International Journal of Science and Research Archive*, vol. 11, no. 1, pp. 350–360, Jan. 2024, doi: 10.30574/ijrsra.2024.11.1.0073.
- [8] S. H. S. Chan, T. Y. Wu, J. C. Juan, and C. Y. Teh, “Recent developments of metal oxide semiconductors as photocatalysts in advanced oxidation processes (AOPs) for treatment of dye waste-water,” Sep. 2011. doi: 10.1002/jctb.2636.
- [9] S. Malato, J. Blanco, A. Vidal, and C. Richter, “Photocatalysis with solar energy at a pilot-plant scale: an overview,” 2002. [Online]. Available: www.psa.es
- [10] P. Cieřła, P. Kocot, P. Mytych, and Z. Stasicka, “Homogeneous photocatalysis by transition metal complexes in the environment,” Dec. 15, 2004. doi: 10.1016/j.molcata.2004.08.043.
- [11] J.-M. Herrmann, “Heterogeneous photocatalysis: fundamentals and applications to the removal of various types of aqueous pollutants,” 1999.
- [12] M. I. Litter, “Heterogeneous photocatalysis Transition metal ions in photocatalytic systems,” 1999.

- [13] S. G. Kumar and L. G. Devi, "Review on modified TiO₂ photocatalysis under UV/visible light: Selected results and related mechanisms on interfacial charge carrier transfer dynamics," Nov. 24, 2011. doi: 10.1021/jp204364a.
- [14] K. Kabra, R. Chaudhary, and R. L. Sawhney, "Treatment of hazardous organic and inorganic compounds through aqueous-phase photocatalysis: A review," Nov. 24, 2004, *American Chemical Society*. doi: 10.1021/ie0498551.
- [15] J. S. Lee and J. Jang, "Hetero-structured semiconductor nanomaterials for photocatalytic applications," Mar. 25, 2014. doi: 10.1016/j.jiec.2013.11.050.
- [16] M. M. Khan, S. F. Adil, and A. Al-Mayouf, "Metal oxides as photocatalysts," Sep. 01, 2015, *Elsevier B.V.* doi: 10.1016/j.jscs.2015.04.003.
- [17] L. Zhang, L. Li, X. Sun, P. Liu, D. Yang, and X. Zhao, "ZnO-layered double hydroxide@graphitic carbon nitride composite for consecutive adsorption and photodegradation of dyes under UV and visible lights," *Materials*, vol. 9, no. 11, 2016, doi: 10.3390/ma9110927.
- [18] S. Porcu, F. Secci, and P. C. Ricci, "Advances in Hybrid Composites for Photocatalytic Applications: A Review," Oct. 01, 2022, *MDPI*. doi: 10.3390/molecules27206828.
- [19] Z. Dong *et al.*, "Raman characterization on two-dimensional materials-based thermoelectricity," 2019, *MDPI AG*. doi: 10.3390/molecules24010088.
- [20] M. Downes *et al.*, "M₅X₄: A Family of MXenes," *ACS Nano*, vol. 17, no. 17, pp. 17158–17168, Sep. 2023, doi: 10.1021/acsnano.3c04967.
- [21] R. M. Ronchi, J. T. Arantes, and S. F. Santos, "Synthesis, structure, properties and applications of MXenes: Current status and perspectives," Oct. 15, 2019, *Elsevier Ltd.* doi: 10.1016/j.ceramint.2019.06.114.
- [22] P. O. Å. Persson and J. Rosen, "Current state of the art on tailoring the MXene composition, structure, and surface chemistry," *Curr Opin Solid State Mater Sci*, vol. 23, no. 6, Dec. 2019, doi: 10.1016/j.cossms.2019.100774.
- [23] M. Hu *et al.*, "Surface Functional Groups and Interlayer Water Determine the Electrochemical Capacitance of Ti₃C₂ T_x MXene," Apr. 24, 2018, *American Chemical Society*. doi: 10.1021/acsnano.8b00676.
- [24] R. M. Ronchi, J. T. Arantes, and S. F. Santos, "Synthesis, structure, properties and applications of MXenes: Current status and perspectives," Oct. 15, 2019, *Elsevier Ltd.* doi: 10.1016/j.ceramint.2019.06.114.
- [25] O. Salim, K. A. Mahmoud, K. K. Pant, and R. K. Joshi, "Introduction to MXenes: synthesis and characteristics," Dec. 01, 2019, *Elsevier Ltd.* doi: 10.1016/j.mtchem.2019.08.010.

- [26] L. Zhang, W. Song, H. Liu, H. Ding, Y. Yan, and R. Chen, “Influencing Factors on Synthesis and Properties of MXene: A Review,” Sep. 01, 2022, *MDPI*. doi: 10.3390/pr10091744.
- [27] L. Verger, C. Xu, V. Natu, H. M. Cheng, W. Ren, and M. W. Barsoum, “Overview of the synthesis of MXenes and other ultrathin 2D transition metal carbides and nitrides,” Jun. 01, 2019, *Elsevier Ltd*. doi: 10.1016/j.cossms.2019.02.001.
- [28] C. E. Shuck *et al.*, “Scalable Synthesis of Ti₃C₂T_x MXene,” *Adv Eng Mater*, vol. 22, no. 3, Mar. 2020, doi: 10.1002/adem.201901241.
- [29] A. Champagne and J. C. Charlier, “Physical properties of 2D MXenes: From a theoretical perspective,” Jul. 01, 2020, *IOP Publishing Ltd*. doi: 10.1088/2515-7639/ab97ee.
- [30] Y. Ibrahim, A. Mohamed, A. M. Abdelgawad, K. Eid, A. M. Abdullah, and A. Elzatahry, “The recent advances in the mechanical properties of self-standing two-dimensional MXene-based nanostructures: Deep insights into the supercapacitor,” Oct. 01, 2020, *MDPI AG*. doi: 10.3390/nano10101916.
- [31] K. A. Papadopoulou, A. Chroneos, D. Parfitt, and S. R. G. Christopoulos, “A perspective on MXenes: Their synthesis, properties, and recent applications,” Nov. 07, 2020, *American Institute of Physics Inc*. doi: 10.1063/5.0021485.
- [32] X. Jiang *et al.*, “Two-dimensional MXenes: From morphological to optical, electric, and magnetic properties and applications,” Mar. 15, 2020, *Elsevier B.V*. doi: 10.1016/j.physrep.2019.12.006.
- [33] L. H. Karlsson, J. Birch, J. Halim, M. W. Barsoum, and P. O. Å. Persson, “Atomically Resolved Structural and Chemical Investigation of Single MXene Sheets,” *Nano Lett*, vol. 15, no. 8, pp. 4955–4960, Aug. 2015, doi: 10.1021/acs.nanolett.5b00737.
- [34] X. H. Zha *et al.*, “The thermal and electrical properties of the promising semiconductor MXene Hf₂CO₂,” *Sci Rep*, vol. 6, Jun. 2016, doi: 10.1038/srep27971.
- [35] K. Huang *et al.*, “Photocatalytic applications of two-dimensional Ti₃C₂MXenes: A review,” Oct. 23, 2020, *American Chemical Society*. doi: 10.1021/acsanm.0c02481.
- [36] A. Szuplewska *et al.*, “Future Applications of MXenes in Biotechnology, Nanomedicine, and Sensors,” Mar. 01, 2020, *Elsevier Ltd*. doi: 10.1016/j.tibtech.2019.09.001.
- [37] S. T. Mahmud *et al.*, “Multilayer MXene Heterostructures and Nanohybrids for Multifunctional Applications: A Review,” Jun. 06, 2022, *American Chemical Society*. doi: 10.1021/acsmaterialslett.2c00175.
- [38] J. Huang, Z. Li, Y. Mao, and Z. Li, “Progress and biomedical applications of MXenes,” *Nano Select*, vol. 2, no. 8, pp. 1480–1508, Aug. 2021, doi: 10.1002/nano.202000309.

- [39] Q. Wang *et al.*, “MXene-based electrochemical (bio) sensors for sustainable applications: Roadmap for future advanced materials,” *Nano Materials Science*, vol. 5, no. 1, pp. 39–52, Mar. 2023, doi: 10.1016/j.nanoms.2022.07.003.
- [40] Y.-Z. Zhang *et al.*, “MXenes stretch hydrogel sensor performance to new limits,” 2018. [Online]. Available: <https://www.science.org>
- [41] J. Zhu *et al.*, “Recent advance in MXenes: A promising 2D material for catalysis, sensor and chemical adsorption,” Dec. 01, 2017, *Elsevier B.V.* doi: 10.1016/j.ccr.2017.09.012.
- [42] M. Xin, J. Li, Z. Ma, L. Pan, and Y. Shi, “MXenes and Their Applications in Wearable Sensors,” Apr. 21, 2020, *Frontiers Media S.A.* doi: 10.3389/fchem.2020.00297.
- [43] L. fei Hong *et al.*, “Recent progress of two-dimensional MXenes in photocatalytic applications: a review,” Dec. 01, 2020, *Elsevier Ltd.* doi: 10.1016/j.mtener.2020.100521.
- [44] K. Huang *et al.*, “Photocatalytic applications of two-dimensional Ti₃C₂MXenes: A review,” Oct. 23, 2020, *American Chemical Society*. doi: 10.1021/acsanm.0c02481.
- [45] N. Dwivedi, C. Dhand, P. Kumar, and A. K. Srivastava, “Emergent 2D materials for combating infectious diseases: The potential of MXenes and MXene-graphene composites to fight against pandemics,” May 07, 2021, *Royal Society of Chemistry*. doi: 10.1039/d1ma00003a.
- [46] N. H. Solangi *et al.*, “MXene as emerging material for photocatalytic degradation of environmental pollutants,” Feb. 15, 2023, *Elsevier B.V.* doi: 10.1016/j.ccr.2022.214965.
- [47] I. Raheem *et al.*, “Rapid growth of MXene-based membranes for sustainable environmental pollution remediation,” Jan. 01, 2023, *Elsevier Ltd.* doi: 10.1016/j.chemosphere.2022.137056.
- [48] N. Liu, N. Lu, Y. Su, P. Wang, and X. Quan, “Fabrication of g-C₃N₄/Ti₃C₂ composite and its visible-light photocatalytic capability for ciprofloxacin degradation,” *Sep Purif Technol*, vol. 211, pp. 782–789, Mar. 2019, doi: 10.1016/j.seppur.2018.10.027.
- [49] T. Wang *et al.*, “Reduced graphene oxide (rGO)/BiVO₄ composites with maximized interfacial coupling for visible light photocatalysis,” *ACS Sustain Chem Eng*, vol. 2, no. 10, pp. 2253–2258, Oct. 2014, doi: 10.1021/sc5004665.
- [50] V. Thirumal *et al.*, “Efficient photocatalytic degradation of hazardous pollutants by homemade kitchen blender novel technique via 2D-material of few-layer MXene nanosheets,” *Chemosphere*, vol. 281, Oct. 2021, doi: 10.1016/j.chemosphere.2021.130984.
- [51] S. Park *et al.*, “Adsorptive and photocatalytic performance of cobalt-doped ZnTiO₃/Ti₃C₂T_x MXene nanohybrids towards tetracycline: Kinetics and mechanistic insight,” *J Hazard Mater*, vol. 443, Feb. 2023, doi: 10.1016/j.jhazmat.2022.130165.

- [52] Z. Chen, Y. Ma, W. Chen, Y. Tang, L. Li, and J. Wang, “Enhanced photocatalytic degradation of ciprofloxacin by heterostructured BiOCl/Ti₃C₂Tx MXene nanocomposites,” *J Alloys Compd*, vol. 950, Jul. 2023, doi: 10.1016/j.jallcom.2023.169797.
- [53] S. Li *et al.*, “A novel MXene-bridged Z-scheme ZnO@Nb₂CTx MXene@carbon nitride nanosheets photocatalyst for efficient enrofloxacin degradation,” *Chemical Engineering Journal*, vol. 489, Jun. 2024, doi: 10.1016/j.cej.2024.151505.
- [54] “Fume hood ‘<https://5.imimg.com/data5/AI/YU/MY-40002218/fume-hood-500x500.jpg>.”
- [55] C. V. Stan, C. M. Beavers, M. Kunz, and N. Tamura, “X-ray diffraction under extreme conditions at the advanced light source,” Mar. 01, 2018, *MDPI*. doi: 10.3390/qubs2010004.
- [56] “Scanning Electron Microscope(SEM) schematic”, <https://nnci.net/seeing-nanoworld>.”
- [57] “EDX,”<https://www.thermofisher.com/blog/materials/edx-analysis-with-sem-how-does-it-work/>.”
- [58] A. Downes and A. Elfick, “Raman spectroscopy and related techniques in biomedicine,” Mar. 2010. doi: 10.3390/s100301871.
- [59] “FTIR,” https://sites.science.oregonstate.edu/~gablek/CH362/bare_irinstrs.htm.”
- [60] “PL spectra,”https://www.researchgate.net/figure/9-Schematic-diagram-of-the-principle-of-PL-spectroscopy_fig9_301789946/download?_tp=eyJjb250ZXh0Ijp7ImZpcnN0UGFnZSI6InB1YmxpY2F0aW9uIiwicGFnZSI6Il9kaXJlY3QifX0.”
- [61] “UV Vis double beam Spectrophotometer,
”https://www.researchgate.net/figure/Schematic-of-UV-Vis-NIR-spectrophotometer_fig24_337902862/download?_tp=eyJjb250ZXh0Ijp7ImZpcnN0UGFnZSI6InB1YmxpY2F0aW9uIiwicGFnZSI6Il9kaXJlY3QifX0.””
- [62] O. Mashtalir, M. R. Lukatskaya, M. Q. Zhao, M. W. Barsoum, and Y. Gogotsi, “Amine-assisted delamination of Nb₂C MXene for li-ion energy storage devices,” *Advanced Materials*, vol. 27, no. 23, pp. 3501–3506, Jun. 2015, doi: 10.1002/adma.201500604.
- [63] Z. Haider *et al.*, “Ag Nanoparticle-Decorated V₂CTx MXene Nanosheets as Catalysts for Water Splitting,” *ACS Appl Nano Mater*, 2022, doi: 10.1021/acsanm.2c04428.
- [64] S. A. Zahra, B. Anasori, M. Z. Iqbal, F. Ravaux, M. Al Tarawneh, and S. Rizwan, “Enhanced electrochemical performance of vanadium carbide MXene composites for supercapacitors,” *APL Mater*, vol. 10, no. 6, Jun. 2022, doi: 10.1063/5.0087457.
- [65] K. Wang, J. Chen, and X. Yan, “MXene Ti₃C₂ memristor for neuromorphic behavior and decimal arithmetic operation applications,” *Nano Energy*, vol. 79, Jan. 2021, doi: 10.1016/j.nanoen.2020.105453.

- [66] I. Ali, S. A. Zahra, I. H. Sajid, and S. Rizwan, "Efficient electrochemical performance of electrostatically self-assembled Nb₂CT_x/AgNPs-CTAB nanocomposite in both basic and neutral electrolytes," *J Energy Storage*, vol. 88, May 2024, doi: 10.1016/j.est.2024.111629.
- [67] R. M. S. Yoo and A. Djire, "Decoupling the Surface and Bulk Reactivities of MXenes and Catalytic Activity Tuning through Surface Chemistry Modification," *ACS Catal*, vol. 13, no. 10, pp. 6823–6836, May 2023, doi: 10.1021/acscatal.3c00655.
- [68] N. Arif, S. Gul, M. Sohail, S. Rizwan, and M. Iqbal, "Synthesis and characterization of layered Nb₂C MXene/ZnS nanocomposites for highly selective electrochemical sensing of dopamine," *Ceram Int*, vol. 47, no. 2, pp. 2388–2396, Jan. 2021, doi: 10.1016/j.ceramint.2020.09.081.
- [69] X. Zhou, Y. Guo, D. Wang, and Q. Xu, "Nano friction and adhesion properties on Ti₃C₂ and Nb₂C MXene studied by AFM," *Tribol Int*, vol. 153, Jan. 2021, doi: 10.1016/j.triboint.2020.106646.
- [70] A. Kudo, R. Niishiro, A. Iwase, and H. Kato, "Effects of doping of metal cations on morphology, activity, and visible light response of photocatalysts," *Chem Phys*, vol. 339, no. 1–3, pp. 104–110, Oct. 2007, doi: 10.1016/j.chemphys.2007.07.024.